

# Global emergence of unprecedented lifetime exposure to climate extremes

<https://doi.org/10.1038/s41586-025-08907-1>

Received: 26 October 2023

Accepted: 17 March 2025

Published online: 7 May 2025

Open access

 Check for updates

Luke Grant<sup>1,2</sup>✉, Inne Vanderkelen<sup>1,3,4</sup>, Lukas Gudmundsson<sup>5</sup>, Erich Fischer<sup>5</sup>, Sonia I. Seneviratne<sup>6</sup> & Wim Thiery<sup>1</sup>

Climate extremes are escalating under anthropogenic climate change<sup>1</sup>. Yet, how this translates into unprecedented cumulative extreme event exposure in a person's lifetime remains unclear. Here we use climate models, impact models and demographic data to project the number of people experiencing cumulative lifetime exposure to climate extremes above the 99.99th percentile of exposure expected in a pre-industrial climate. We project that the birth cohort fraction facing this unprecedented lifetime exposure to heatwaves, crop failures, river floods, droughts, wildfires and tropical cyclones will at least double from 1960 to 2020 under current mitigation policies aligned with a global warming pathway reaching 2.7 °C above pre-industrial temperatures by 2100. Under a 1.5 °C pathway, 52% of people born in 2020 will experience unprecedented lifetime exposure to heatwaves. If global warming reaches 3.5 °C by 2100, this fraction rises to 92% for heatwaves, 29% for crop failures and 14% for river floods. The chance of facing unprecedented lifetime exposure to heatwaves is substantially larger among population groups characterized by high socioeconomic vulnerabilities. Our results call for deep and sustained greenhouse gas emissions reductions to lower the burden of climate change on current young generations.

Climate extremes have detrimental effects on society and are a foremost concern around climate change<sup>1</sup>. Anthropogenic influences have been identified in heatwaves, river floods, droughts, crop failures and certain aspects of wildfires and tropical cyclones<sup>2,3</sup>. With continued atmospheric warming, the intensity, frequency and duration of some of these events are projected to increase further<sup>4–9</sup>, with varying levels and spread depending on the event considered<sup>3</sup>. Current policies could warm global mean temperature (GMT) to +2.7 °C (+2.2–3.4 °C) above pre-industrial levels by the end of the century<sup>10</sup>. As this warming is expected to increase human exposure to climate extremes<sup>3</sup>, young generations will reap the consequences of the present-day mitigation of greenhouse gas emissions.

The above climate extremes are projected to occur most frequently across the lifetimes of current young generations<sup>11</sup>. As such, the number of climate extremes experienced across a person's lifetime can far exceed the expected exposure under a pre-industrial climate. Yet, the number of people who will experience this unprecedented lifetime exposure (ULE) to climate extremes remains unclear. Here we cross an extensive portfolio of multi-model projections of climate extremes with demographic data, GMT trajectories and two measures of vulnerability. We evaluate the emergence of ULE to extreme events at the grid scale to estimate the global membership of birth cohorts that will face ULE (Methods). Then, we show how this sub-population is stratified in terms of vulnerability. This is one of the first estimates of the number of people projected to experience ULE across a multidimensional framework, including birth year, warming scenario and vulnerability.

## Unprecedented exposure to heatwaves

We illustrate what ULE means for extreme heatwaves in one grid cell ( $0.5^\circ \times 0.5^\circ$ ) located over Brussels, Belgium, for three GMT pathways in which warming above pre-industrial temperatures reaches 1.5 °C, 2.5 °C and 3.5 °C by the year 2100. People born in 1960 and spending their life in Brussels are projected to experience three heatwaves in their lifetime, showing little sensitivity to the GMT pathway (Fig. 1a). In this location, the 1960 birth cohort does not exceed the threshold of ULE, which we define as the 99.99th percentile of a large sample of lifetime exposures in a pre-industrial control climate and which is six heatwaves here (Fig. 1b, grey histogram and dashed line). By contrast, the 1990 birth cohort emerges into ULE for the two warmest GMT pathways shown (Fig. 1c,d). This implies that, under temperature pathways reaching 2.5 °C or higher warming by 2100, this cohort will face more heatwaves than they would have been expected to experience with a one in ten thousand chance in the absence of climate change. Different GMT pathways cause a further divergence in the lifetime exposure of those born in 2020 in this location (Fig. 1e,f). In the 1.5 °C pathway, the 2020 birth cohort is projected to experience nearly 11 heatwaves, yet this increases to 18 and 26 heatwaves in pathways reaching 2.5 °C and 3.5 °C, respectively, by the end of the century. This by far exceeds the ULE threshold under each GMT pathway, with an age of emergence already around 40 years old for the 2.5 °C and 3.5 °C pathways (Fig. 1e). We then count the number of people per birth cohort that eventually reach ULE, using absolute population estimates at the grid scale and

<sup>1</sup>Department of Water and Climate, Vrije Universiteit Brussel, Brussels, Belgium. <sup>2</sup>Canadian Centre for Climate Modelling and Analysis, Environment and Climate Change Canada, Victoria, British Columbia, Canada. <sup>3</sup>Department of Earth and Environmental Sciences, KU Leuven, Leuven, Belgium. <sup>4</sup>Royal Meteorological Institute Belgium, Brussels, Belgium. <sup>5</sup>Institute for Atmospheric and Climate Science, ETH Zurich, Zurich, Switzerland. <sup>✉</sup>e-mail: luke.grant@ec.gc.ca

# 前所未有的终身暴露于气候极端的全球出现

<https://doi.org/10.1038/s41586-025-08907-1>

收到：2023年10月26日

接受：2025年3月17日

在线发布：2025年5月7日

开放访问

 检查更新

Luke Grant<sup>1,2</sup>, Inne Vanderkelen<sup>1,3,4</sup>, Lukas Gudmundsson<sup>5</sup>, Erich Fischer<sup>5</sup>, Sonia I. Seneviratne<sup>5</sup>和Wim Thiery<sup>1</sup>

在人为气候变化<sup>1</sup>下，极端气候正在升级。但是，这如何转化为一个人一生中前所未有的累积极端事件暴露尚不清楚。在这里，我们使用气候模型，影响模型和人口统计数据来投射经历累积终身暴露的人数，以高于前工业气候中预期的暴露量高于99.99%的极端。我们预计，面对这种前所未有的终身暴露于热浪，农作物故障，河流洪水，干旱，野火，野火和热带气旋的终身暴露量，从1960年到2020年将至少翻一番，并在当前的缓解政策与 $2.7^{\circ}\text{C}$ 以上的全球暖途径相一致，而Pre-c after-predy a}  $^{\circ}\text{C}$ 以上的预定量为2100。1.  $5^{\circ}\text{C}$ 途径，2020年出生的人中有52%会经历前所未有的终身暴露于热浪。如果全球变暖达到 $3.5^{\circ}\text{C}$  2100，则热浪的级数上升到92%，农作物衰竭29%，河流洪水量增加14%。在以高社会经济脆弱性为特征的人群中，面对前所未有的终身暴露的机会大大更大。我们的结果要求减少深层和持续的温室气体排放，以降低当前年轻人的气候变化负担。

极端气候对社会产生不利影响，对气候变化<sup>1</sup>的最大关注。在热浪，河流洪水，干旱，农作物失败以及野火和热带气旋的某些方面<sup>2,3</sup>中已经确定了人为影响。随着大气变暖的持续，预计其中一些事件的强度，频率和持续时间将进一步增加<sup>4-9</sup>，随着LEV-EL的变化，并取决于被认为<sup>3</sup>的事件。当前的策略可以将全球平均温度（GMT）加热到 $+2.7^{\circ}\text{C}$  ( $+2.2\text{--}3.4^{\circ}\text{C}$ ) 到本世纪末<sup>10</sup>之前的工业前水平以上。由于预计这种变暖将增加人类对极端气候的暴露<sup>3</sup>，年轻一代将收获当今缓解温室气体排放的后果。

预计在当前年轻一代<sup>11</sup>的一生中，上述极端极端的发生。因此，在一个人的一生中经历的极端气候极端可能远远超出了工业前气候下的预期暴露。然而，将遇到这种空前的终身暴露（ULE）的人数尚不清楚。在这里，我们通过人口统计数据，GMT轨迹和两种脆弱能力的措施，超过了气候极端的多模型投影的广泛投资组合。我们评估了ULE到极端事件的出现，以估计面对ULE的全球出生队列成员资格（方法）。然后，我们展示了如何根据脆弱性对该子人口进行分层。这是预计将在多维框架中体验ULE的人数的首次估计之一，包括出生年份，变暖场景和脆弱性。

## 空前接触热浪

我们说明了一个网格电池中极端热浪的含义 ( $0.5^{\circ} \times 0.5^{\circ}$ )，位于比利时布鲁塞尔的三种GMT途径上，在三种GMT途径中，在工业前温度上方的温度达到 $1.5^{\circ}\text{C}$ ,  $2.5^{\circ}\text{C}$ 和 $3.5^{\circ}\text{C}$  and and Inluptive pation。预计他们在布鲁塞尔的生活将在他们的一生中体验三个热浪，对GMT途径几乎没有敏感性（图 1A）。在这个位置，1960年的出生队列不超过ULE的阈值，我们将其定义为前工业前控制气候中大量终生暴露的第99.99个百分点，在这里是六个热浪（图。相比之下，1990年的出生队列出现在ULE中，以显示两个最温暖的GMT路径（图 1C, D）。这意味着，在达到 $2.5^{\circ}\text{C}$ 或更高变暖的温度路径下，到2100年，该队列将面临比在没有气候变化的情况下会有一万分之一的机会所带来的热浪。不同的GMT途径在2020年在该位置出生的人的生命周期暴露导致进一步的差异（图 1E, F）。在 $1.5^{\circ}\text{C}$ 途径中，2020年出生队列预计将经历近11个热浪，但在本世纪末，这将增加到18和26热波，分别达到 $2.5^{\circ}\text{C}$ 和 $3.5^{\circ}\text{C}$  and  $3.5^{\circ}\text{C}$ 。到目前为止，这超过了每个GMT途径下的ULE阈值，在 $2.5^{\circ}\text{C}$  and  $3.5^{\circ}\text{C}$ 途径的出现年龄大约为40岁的年龄（图 1E）。然后，我们使用网格量表的绝对人口估算值来计算最终到达ULE的每个人数的人数

<sup>1</sup>Department of Water and Climate, Vrije Universiteit Brussel, Brussels, Belgium. <sup>2</sup>Canadian Centre for Climate Modelling and Analysis, Environment and Climate Change Canada, Victoria, British Columbia, Canada. <sup>3</sup>Department of Earth and Environmental Sciences, KU Leuven, Leuven, Belgium. <sup>4</sup>Royal Meteorological Institute Belgium, Brussels, Belgium. <sup>5</sup>Institute for Atmospheric and Climate Science, ETH Zurich, Zurich, Switzerland. <sup>✉</sup>e-mail: luke.grant@ec.gc.ca

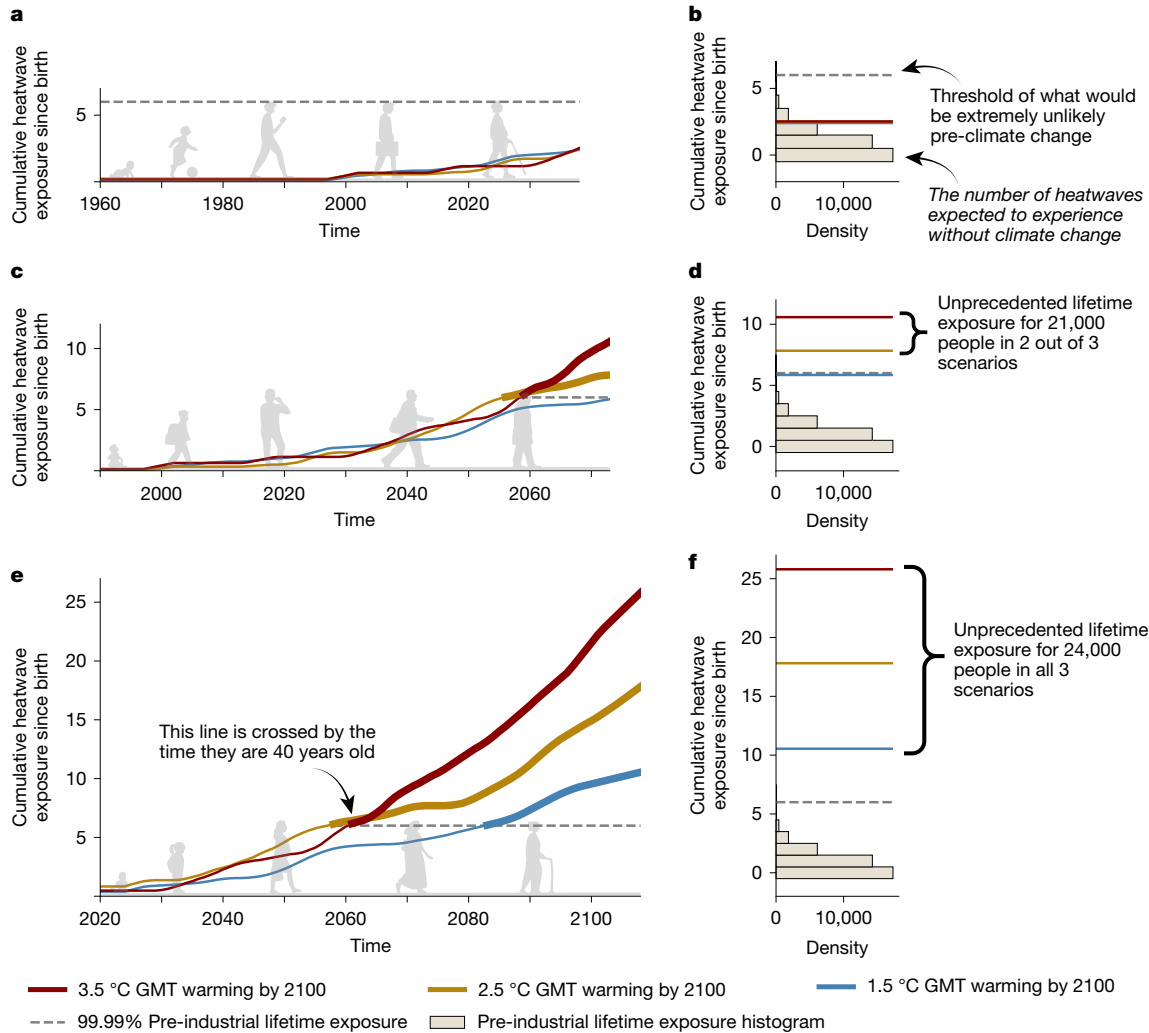


**Fig. 1 | CUMULATIVE HEATWAVE EXPOSURE SINCE BIRTH FOR BRUSSELS, BELGIUM.**

**a,c,e**, Multi-model mean time series of cumulative heatwave exposure for people born in 1960 (**a**), 1990 (**c**) and 2020 (**e**) in 1.5 °C (blue line), 2.5 °C (gold line) and 3.5 °C (red line) pathways. **b,d,f**, Histograms for 1960 (**b**), 1990 (**d**) and 2020 (**f**) birth cohorts show the pre-industrial sample density of 40,000 bootstrapped lifetime exposures overlaid with final lifetime exposures from the time series of

the birth cohort. Dashed lines show the 99.99th percentile of the pre-industrial sample distribution, that is, the threshold of unprecedented lifetime exposure (ULE) for this location, cohort and climate extreme. Counts of people (right of **d,f**) show the population of the birth cohort that has emerged beyond the 99.99th percentile of the pre-industrial sample distribution.

relative cohort sizes at the country level. In this location, a best estimate of 21,000 people from the 1990 birth cohort and 24,000 people from the 2020 birth cohort are projected to experience ULE (except for the 1990 birth cohort under the 1.5 °C pathway). Under a 1.5 °C pathway, all cohorts born in Brussels after 1990 reach ULE, totalling 665,000 people. For a 3.5 °C pathway, ULE begins for people born in 1978, increasing this total to 941,000 people. For cohorts that emerge, it is virtually certain (at least >99.99% chance) that their lifetime heatwave exposure cannot be explained by internal climate variability.

We now repeat this analysis for every land grid cell and project the population fraction of each birth cohort experiencing ULE to heatwaves across the globe ( $CF_{heatwaves}$  for cohort fraction reaching ULE to heatwaves). Of the 81 million people born in 1960, on average, around 16% (13 million people) face ULE to heatwaves regardless of the scenario. This fraction rises towards younger generations, and from the 1980 birth cohort onwards,  $CF_{heatwaves}$  begins to depend on GMT pathways (Fig. 2a). In a 1.5 °C pathway,  $CF_{heatwaves}$  stabilizes for recent birth cohorts, reaching an average of 52% for the 2020 birth cohort (62 million people). Comparatively,  $CF_{heatwaves}$  of the 2020 birth cohort is almost doubled in a 3.5 °C pathway, reaching 92%. This implies that 111 million children born in 2020 will live an unprecedented life in terms of heatwave

exposure in a world that warms to 3.5 °C compared with 62 million in a 1.5 °C pathway.

At the country level,  $CF_{heatwaves}$  for the 2020 birth cohort is the highest in the tropics under low GMT pathways, yet this pattern disappears as heatwaves become widespread under high GMT pathways (Fig. 2c–e and Supplementary Tables 1–3). Under a 1.5 °C pathway, equatorial regions have relatively high  $CF_{heatwaves}$ ; of the 177 countries in this analysis, 104 have most of the population of 2020 birth cohort living with unprecedented exposure to heatwaves ( $CF_{heatwaves} \geq 50\%$ ; Fig. 2c). This latitudinal pattern is less apparent in a 2.5 °C pathway (Fig. 2d). Here, 157 countries have  $CF_{heatwaves} \geq 50\%$ . In a 3.5 °C pathway, 167 countries have  $CF_{heatwaves} \geq 50\%$ , 155 countries have  $CF_{heatwaves} \geq 90\%$  and in 113 countries the entire birth cohort faces unprecedented heatwave exposure ( $CF_{heatwaves} = 100\%$ ; Fig. 2e).

## Unprecedented multi-hazard exposure

We then expand the analysis to a total of six climate extremes<sup>12</sup> and 21 warming pathways (Fig. 3 and Methods). For every combination of birth cohort, climate extreme and warming pathway, we quantify the number of people experiencing ULE at the grid scale and subsequently

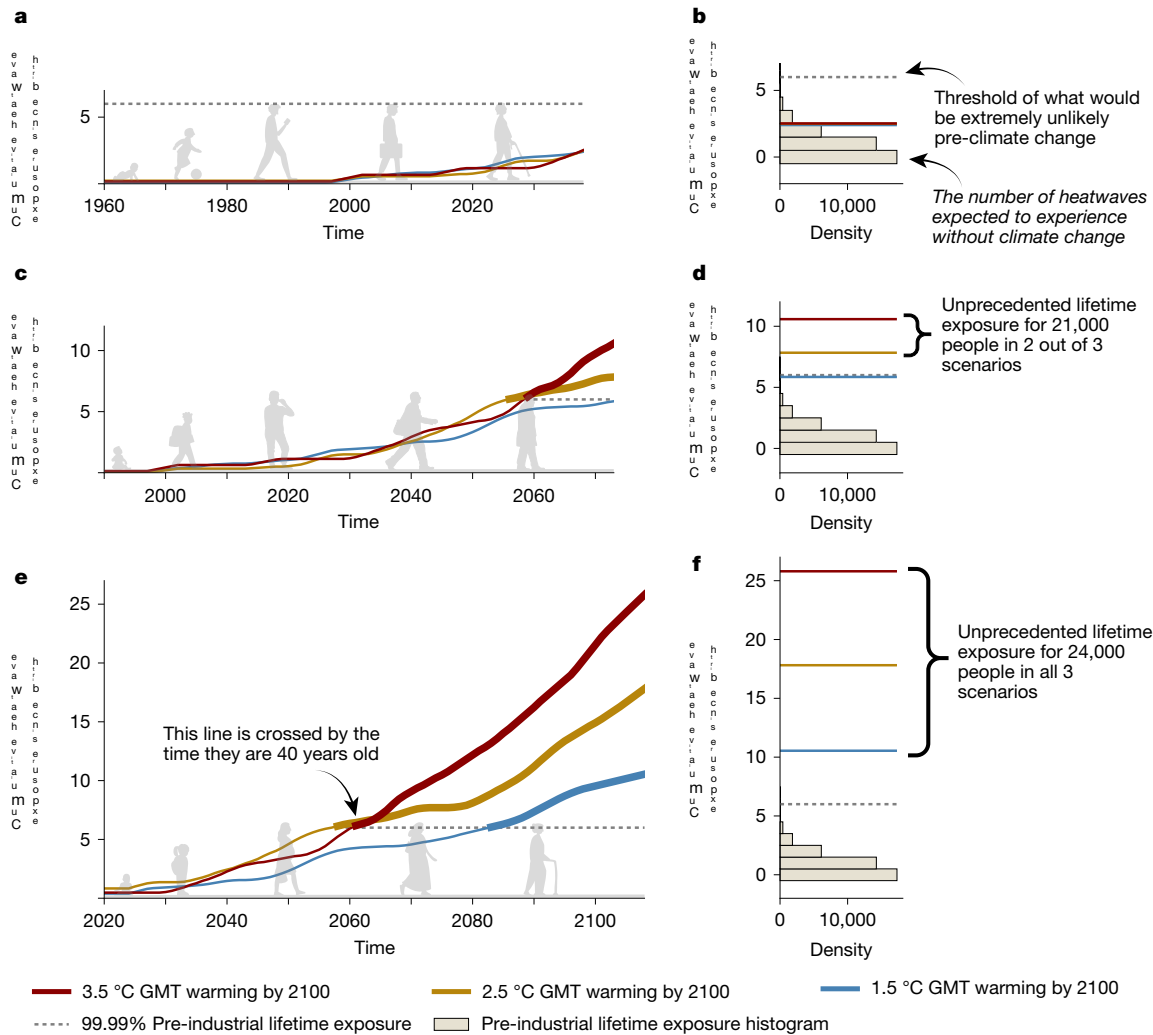


图1 | 比利时布鲁塞尔出生以来的累积热波暴露。A, C, E, 为1960年(A), 1990年(C)和2020(e)的累积热量暴露的多模型平均时间序列, 1.5 °C(蓝线), 2.5 °C(金线)和3.5 °C(v35)°C(红线)。B, D, F, 1960(b), 1990(d)和2020(f)出生队列的直方图显示, 工业前样品密度的40,000个自举的终身暴露覆盖了覆盖的终身暴露, 并从出生队列的时间序列中进行了最终的终身暴露。虚线显示了该位置, 同类和气候极端的前所未有的寿命暴露(ULE)的阈值, 即前所未有的寿命暴露(ULE)的阈值。人数(D, f)的人数显示出出现的出生队列的人口, 该人群已经超过了工业前样本分布的第99.99%的机会。

相对队列的大小在国家一级。在这个位置, 预计1990年出生队列的21,000人和2020年出生队列的24,000人的最佳估计预计将体验ULE(根据1.5 °C途径, 1990年的出生队列除外)。在1.5 °C途径下, 所有人群都在1990年后出生在布鲁塞尔, 到达ULE, 总计66.5万人。对于3.5 °C的途径, ULE开始为1978年出生的人们开始, 将这一总数增加到941,000人。对于出现的队列, 实际上(至少>99.99%的机会)可以通过内部气候变异性来解释它们的寿命热波暴露。

现在, 我们重复每个土地网格电池的分析, 并将每个出生队列的人口分数投射到全球的热浪中( $CF_{heatwaves}$ , 用于群体, 以达到ULE到热波)。在1960年出生的8100万人中, 无论情况如何, 这一比例向年轻一代上升, 从1980年的出生队列开始,  $CF_{heatwaves}$ 开始依赖GMT途径(图2a)。在1.5 °C途径中,  $CF_{heatwaves}$ 稳定了最近的出生队列, 平均达到2020年出生队列(6200万人)的平均52%。相比之下, 2020年出生队列的 $CF_{heatwaves}$ 在3.5 °C途径中几乎翻了一番, 达到92%。这意味着2020年出生的1.11亿个孩子将在Heatwave上过着前所未有的生活。

在一个温暖到3.5 °C的世界中的暴露, 而6200万1.5 °C途径。

在国家一级, 对于2020年出生队列的 $CF_{heatwaves}$ 在低GMT途径下是热带地区最高的, 但是随着热浪在高GMT途径下的广泛影响, 这种模式消失了(图2a)。在1.5 °C途径下, 赤道区域的 $CF_{heatwaves}$ 相对较高; 在该分析中的177个国家中, 有104个人口的2020年人口大部分人口居住着前所未有的热波接触( $cf_{heatwaves} \geq 50\%$ ; 图2c)。在2.5 °C途径中, 这种纬度模式较不明显(图2d)。在这里, 157个国家/地区的 $CF_{heatwaves} \geq 50\%$ 。在3.5 °C途径中, 167个国家/地区具有 $CF_{heatwaves} \geq 50\%$ , 155个国家的 $CF_{heatwaves} \geq 90\%$ , 在113个国家中, 整个出生的同类群体面临着前所未有的热量曝光( $CF_{heatwaves} = 100\%$ ); 图2e)。

### 空前的多危险暴露

然后, 我们将分析扩展到总共六个气候极端<sup>12</sup>和21个变暖途径(图3和方法)。对于出生队列, 气候极端和温暖途径的每一个组合, 我们量化了在网格尺度上经历ULE的人数。

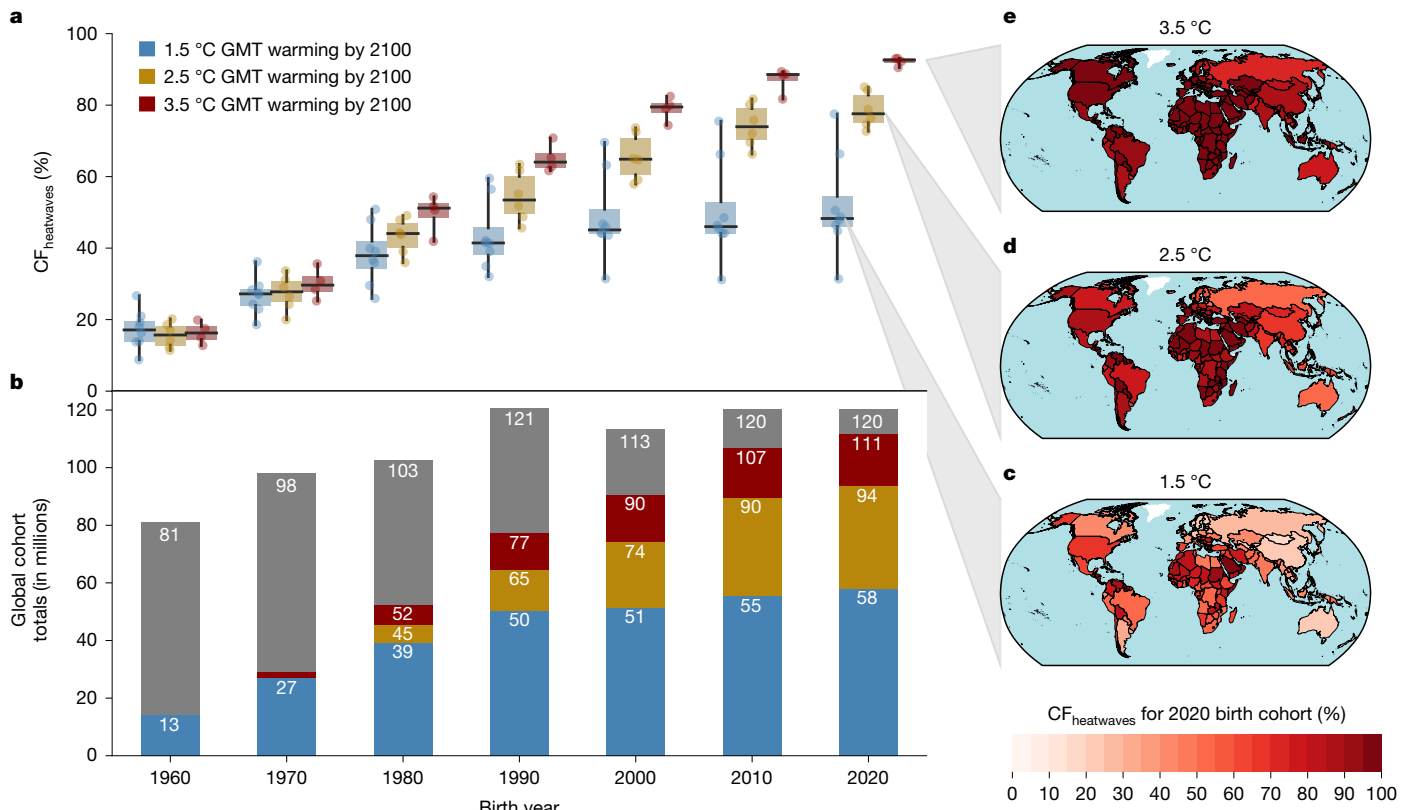


**Fig. 2 | Rising fraction of birth cohorts facing unprecedented lifetime heatwave exposure.** **a**, Box plots show the cohort fraction reaching ULE to heatwaves (CF<sub>heatwaves</sub>) for 1.5 °C (blue), 2.5 °C (gold) and 3.5 °C (red) pathways for global birth cohorts between 1960 and 2020 (middle line, median; box limits, upper and lower quartiles; whiskers, extend to the full range of the

model ensemble). **b**, Bars show global cohort sizes in millions, with totals in grey and median numbers of people reaching ULE to heatwaves for 1.5 °C (blue), 2.5 °C (gold) and 3.5 °C (red) pathways. **c–e**, Maps display country-level CF<sub>heatwaves</sub> of the 2020 birth cohort for 1.5 °C (**c**), 2.5 °C (**d**) and 3.5 °C (**e**) pathways.

aggregate to the country or global level. Cohort fraction (CF) for climate extremes other than heatwaves is lower across all birth years and GMT pathways because they are generally less widespread than heatwaves; however, they still affect a large population fraction (Fig. 3 and Supplementary Tables 4–18). In a 3.5 °C pathway, 29% of those born in 2020 will live through unprecedented exposure to crop failures (Fig. 3b). This is followed by river floods, in which 14% will face unprecedented exposure to this extreme (Fig. 3e). As not all climate projections reach high warming levels, the ensemble size shrinks towards higher warming levels. Consequently, crop failures, droughts, river floods and tropical cyclones, which are more dependent on changes in the water cycle than heatwaves, exhibit discontinuities in CF at some GMT intervals (Fig. 3b,d–f). These sampling artefacts disappear when visualizing CFs for a smaller subset of simulations that are available for all GMT trajectories (Supplementary Note 1 and Supplementary Fig. 1). Although model uncertainties are larger for extremes other than heatwaves, differences in CF across birth cohorts are statistically significant for all six climate extremes (Supplementary Note 2 and Supplementary Figs. 2 and 3).

Across all projections available for the 2.7 °C pathway aligned with current policies<sup>10</sup>, ULE to heatwaves occurs in the Americas, Africa, the Middle East and Australia already for the 1960 birth cohort and globally for the 2020 birth cohort (Supplementary Figs. 4m–o and 5e,k). The ULE to crop failures expands around the United States, South America, Sub-Saharan Africa and East Asia between 1960 and 2020 cohorts (Supplementary Figs. 4 and 5b,h). The ULE to river floods occurs in northern latitudes for the 1960 cohort, in line with the observations and model projections for precipitation changes<sup>13–15</sup> and expands southwards into much of the world for the 2020 cohort (Supplementary Fig. 5d,j).

The lower CF of some extremes, such as tropical cyclones, is expected given the geographical constraints of these events and their distinct meteorological drivers. Tropical cyclones can, therefore, be re-evaluated by limiting the analysis to regions that can experience them. We consider these regions to be any grid cells exposed at least once to the event across our whole ensemble of exposure projections (Supplementary Fig. 6). CF<sub>tropical cyclones</sub> nearly doubles when constraining total birth cohort size to exposed regions. For the 2020 birth cohort, this estimate changes from 6% to 11% in a 1.5 °C pathway and from 10% to 19% in a 3.5 °C pathway.

## Heatwaves across vulnerability strata

Finally, we cross our grid-scale projections for ULE to heatwaves against two grid-scale indicators of socioeconomic vulnerability (Methods): (1) the Global Gridded Relative Deprivation Index v.1 (GRDI; ref. 16), which expresses relative deprivation according to six socioeconomic indicators; and (2) lifetime mean GDP per capita (denoted as GDP; ref. 17). Binning our birth cohort members into the top and bottom 20% of GRDI (Fig. 4a) and GDP (Supplementary Fig. 7a) enables a grid-scale comparison of ULE for population groups with high and low socioeconomic vulnerability. Using GRDI, we find that the most vulnerable subset of each birth cohort projected to experience ULE to heatwaves under current policies is substantially larger than the least vulnerable subset. This implies that socioeconomically vulnerable people have a consistently higher chance of facing unprecedented lifetime heatwave exposure compared with the least vulnerable members of their generation (Fig. 4b). For example, of the 2020 birth cohort, 95% or 23 million members of the high deprivation (high socioeconomic vulnerability)

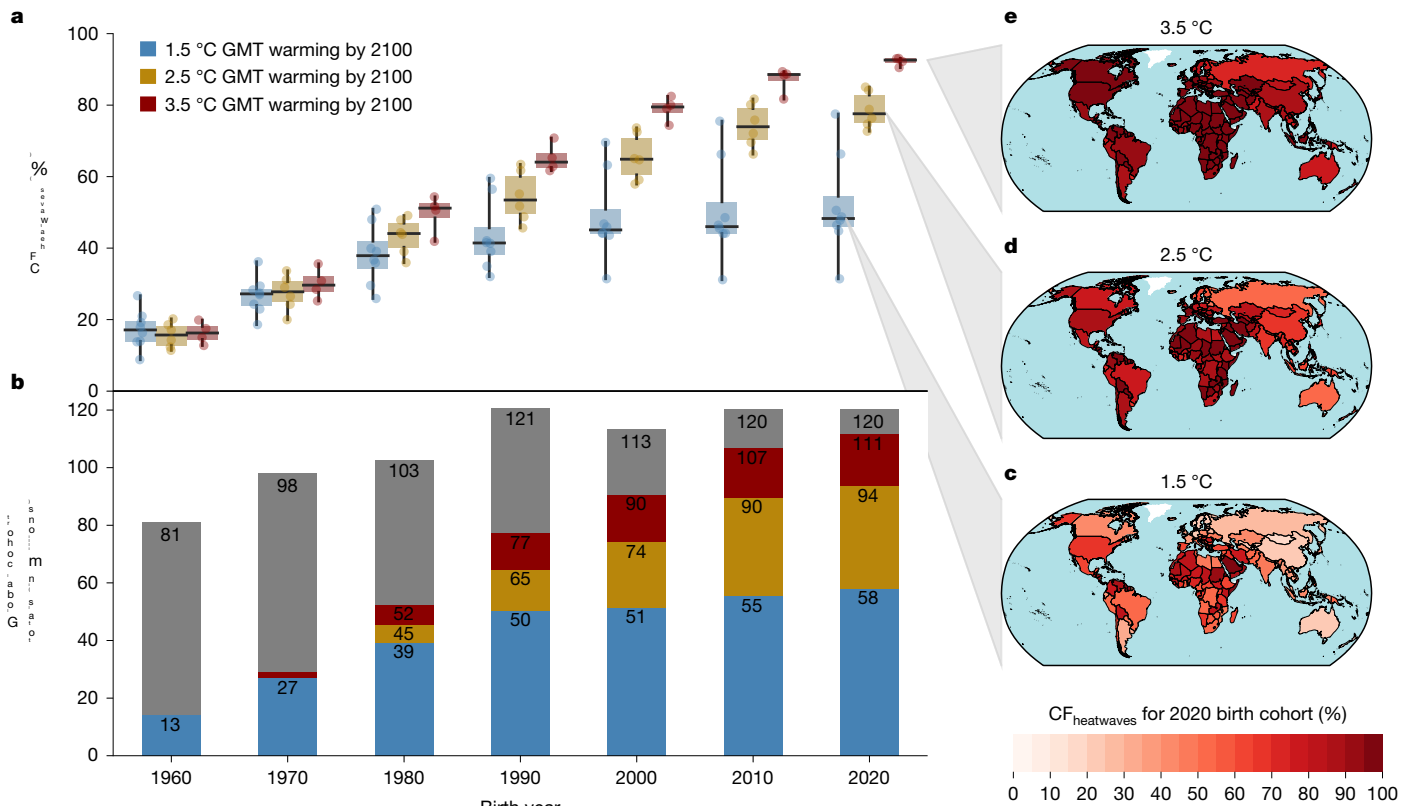


图2 | 面对前所未有的终身热浪暴露的出生队列的上升。a，盒子图显示了1.5 °C (blue)，2.5 °C (gold) 和3.5 °C (red)之间的全球出生群体，在1960年和2020年之间，quartiles umedian umipers;模型合奏的全范围）。B，杆显示全球队列的大小数百万，总数为灰色，中位数人以1.5 °C (蓝色)，2.5 °C (黄金) 和3.5 °C (红色) 途径的中位数。C – E，图显示为1.5 °C (c)，2.5 °C (d) 和3.5 °C (e) 途径的2020年出生队列的国家级别CF<sub>heatwaves</sub>。

汇总到该国或全球一级。在所有出生年份和GMT途径中，除热浪以外的气候极端的队列分数 (CF)，因为它们通常不如热浪传播。但是，它们仍然会影响较大的人口分数 (图 3和补充表 4–18)。在3.5 °C途径中，2020年出生的人中有29%将通过前所未有的作物衰竭来生活 (图 3 b)。其次是河流洪水，其中14%将面临前所未有的暴露于这种极端 (图 3E)。由于并非所有的气候预测达到高变暖水平，因此整体尺寸缩小了更高的变暖水平。因此，与热浪相比，农作物失败，干旱，河流洪水和热带气旋更依赖于水周期的变化，在某些GMT间隔内表现出CF的不连续性 (图 3B, D – F)。当可视化CFS的较小的模拟子集时，这些采样伪像消失了，这些模拟可用于所有GMT轨迹 (补充注释 1和补充图。图 1)。尽管模型的不确定性对于热浪以外的极端情况更大，但对于所有六个气候极端，跨出生队列的CF差异在统计学上都是显着的 (补充说明 2和补充无花果。 2和3)。

在2.7 °C的所有预测中，与当前的政策<sup>10</sup>一致，ule到热浪发生在美洲，非洲，非洲，中东，中东和澳大利亚已经在1960年出生的同龄人和2020年出生队列的全球群体 (补充无花果。在1960年至2020年之间，农作物失败在美国，南美洲，撒哈拉以南非洲和东亚地区扩展 (补充无花果。 4和5b, h)。ule到河洪水发生在1960年的北纬度地区，这与降水变化的观察值和模型预测<sup>13–15</sup>一致，并在2020年群体 (sup-plentyary sup-lentary图5D, j)中向南扩展到世界上的大部分地区。

鉴于这些事件的地理约束及其独特的气象驱动因素，预计某些极端的CF (例如热带气旋)。因此，可以通过将分析限制为可以体验它们的区域来重新评估热带气旋。我们认为这些区域是在整个暴露投影整体中至少暴露于事件中一次的任何网格单元 (补充图 6)。当将总出生队列大小限制为暴露区域时，CF<sub>tropical cyclones</sub>几乎翻了一番。对于2020年的出生队列，该估计在1.5 °C途径中从6%变为11%，在3.5 °C途径中从10%变为10%。

### 遍布脆弱性层的热浪

最后，我们对Ule的网格尺度投影，以与两个网格尺度的社会经济脆弱性指标 (方法)：(1) 全球栅格相对剥夺指数v.1 (grdi; ref; ref。 16)，根据六个社会经济学指标表达相对剥夺，这表明相对剥夺。(2) 寿命平均人均GDP人均GDP (称为GDP;参考 17)。将我们的出生队列成员纳入GRDI的顶部和底部的20% (图 4A) 和GDP (补充图。图 7A) 可以使ULE的网格规模比较高和低社会经济脆弱性。使用Grdi，我们发现，根据当前政策，预计将在热浪中体验到热浪的每个出生队列中最脆弱的子集大大比最小脆弱的子集大。这意味着与最脆弱的属性成员相比，社会经济上脆弱的人始终面临前所未有的终身热浪暴露的机会 (图 4b)。例如，在2020年出生队列中，有95%或2300万成员高剥夺 (高社会经济脆弱性)

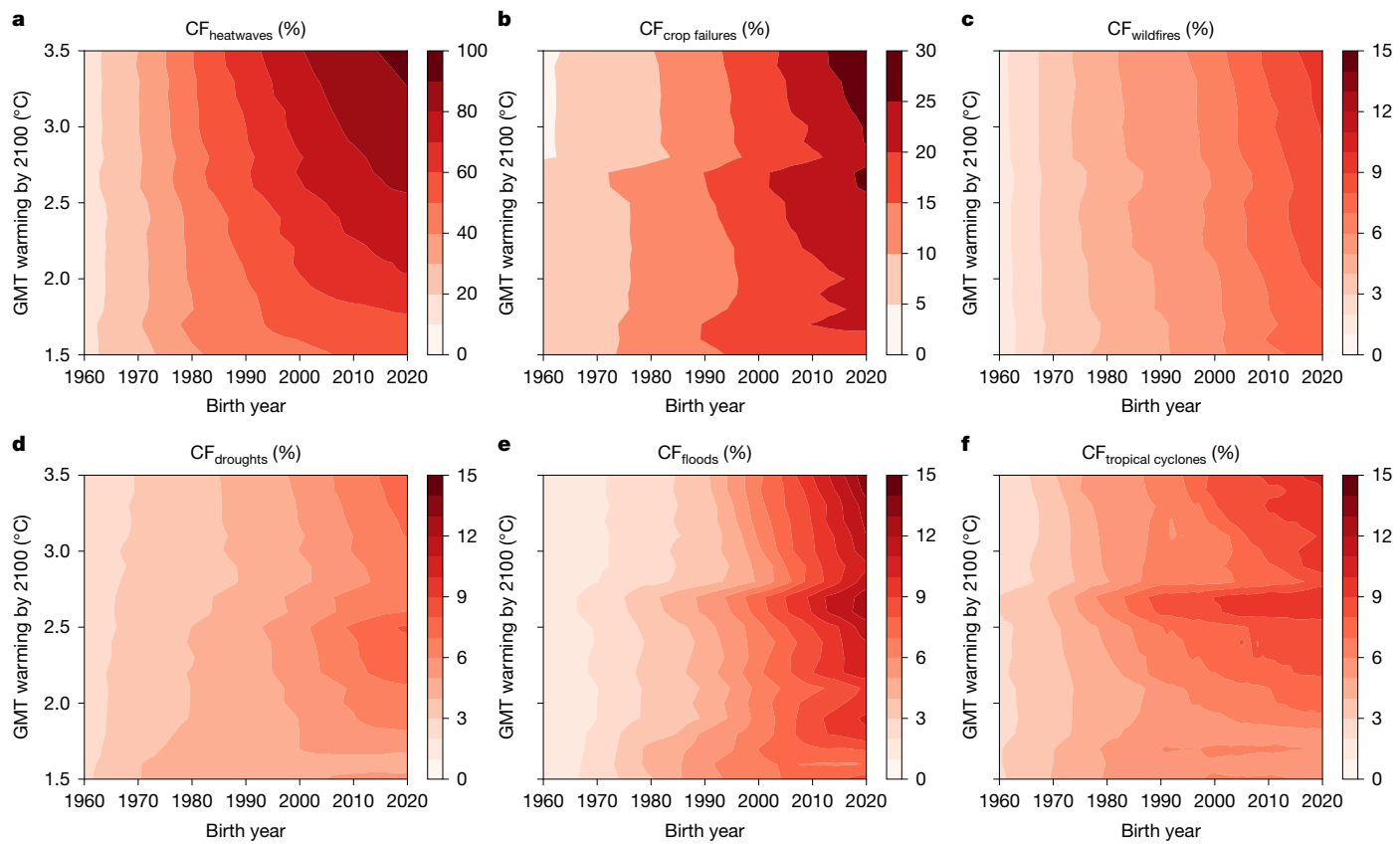


**Fig. 3 | Greater unprecedented exposure to climate extremes for younger generations and higher warming pathways.** **a–d**, Cohort fraction (CF) across all birth years (1960–2020) and GMT pathways (1.5–3.5 °C) for heatwaves

(CF<sub>heatwaves</sub>; **a**), crop failures (CF<sub>crop failures</sub>; **b**), wildfires (CF<sub>wildfires</sub>; **c**), droughts (CF<sub>droughts</sub>; **d**), river floods (CF<sub>floods</sub>; **e**) and tropical cyclones (CF<sub>tropical cyclones</sub>; **f**). Each extreme event panel has its colour bar range.

group face ULE to heatwaves, whereas this is 78% (19 million) for the low deprivation group. This disparity is similar when using GDP, but with only 1974 and later birth years having significant differences across vulnerability strata (Supplementary Fig. 7). Here, for the 2020 birth year, 92% (22 million) of the low-income group face ULE under current policies, whereas this is 79% (19 million) for the high-income group. Under alternative warming pathways of 1.5 °C and 3.5 °C, although the same direction of disparities remains across vulnerability strata, the lowest vulnerability groups (low deprivation and high GDP) benefit the most from a low warming pathway (Fig. 4c,d and Supplementary Fig. 7c,d). Socioeconomically vulnerable groups have lower adaptive capacity and face more constraints when it comes to implementing effective adaptation measures<sup>18,19</sup>. Our results highlight that precisely these groups with the highest socioeconomic vulnerability and lowest adaptation potential face the highest chance for unprecedented heatwave exposure (Fig. 4). This underlines the disproportionate risk for deprived communities in light of past and future climate extremes.

## Discussion

Our analysis only quantifies local exposure by design; yet in reality, the effects of climate extremes cascade non-locally. For example, in 2023, smoke from an active wildfire season in Canada was transported south along the east coast of the United States, exposing millions of people to hazardous air quality<sup>20</sup> and causing an increased cardiopulmonary disease burden<sup>21</sup>. Climate extremes also affect society through economic impacts, including the rising cost of living due to supply chain disruptions<sup>22</sup> and taxation to recover public infrastructure<sup>23</sup>. For instance, climate change endangers staple crop production in

the main breadbasket countries that supply most of our caloric intake globally<sup>24</sup>, forcing market instabilities that only the wealthiest can cope with<sup>25</sup>. These missing non-local impacts make our estimates conservative.

By contrast, we do not capture how people adapt to extremes and thereby potentially reduce their exposure or vulnerability. For example, exposure to heatwaves can be reduced for population groups that can afford access to air conditioning<sup>18</sup>. However, maladaptive responses to climate extremes can instead create lock-ins of vulnerability and exposure<sup>1</sup>. Therefore, our lifetime exposure estimates omit beneficial adaptation outcomes as well as detrimental non-local and maladaptation effects. Finally, opting for a threshold below 99.99% would lower the bar and increase ULE estimates, and vice versa. Yet this effect is limited because the reference distribution is typically composed of small integers. By contrast, using thresholds above 99.99% risks redundancy in our bootstrapped data sample (Methods).

Some demographic realities are not accounted for here. Factors such as within-country migration, fertility and mortality respond in reality to the climate extremes considered here<sup>11</sup>. In the United States, where the population faces exposure to all extremes analysed in this study, city centres attract young people<sup>26</sup> and disparities in life expectancy have been found across race–county combinations<sup>27</sup> and rural–urban residency<sup>28</sup>. For instance, life expectancy is longer for those living in cities, yet here we apply country-average life expectancy and cohort size distribution uniformly within each country. Furthermore, we do not account for within-grid-cell heterogeneity, that is, we miss some fine-scale variations in socioeconomic vulnerability and exposure in socioeconomically diverse regions such as cities. Finally, we focus on the socioeconomic dimension of vulnerability,

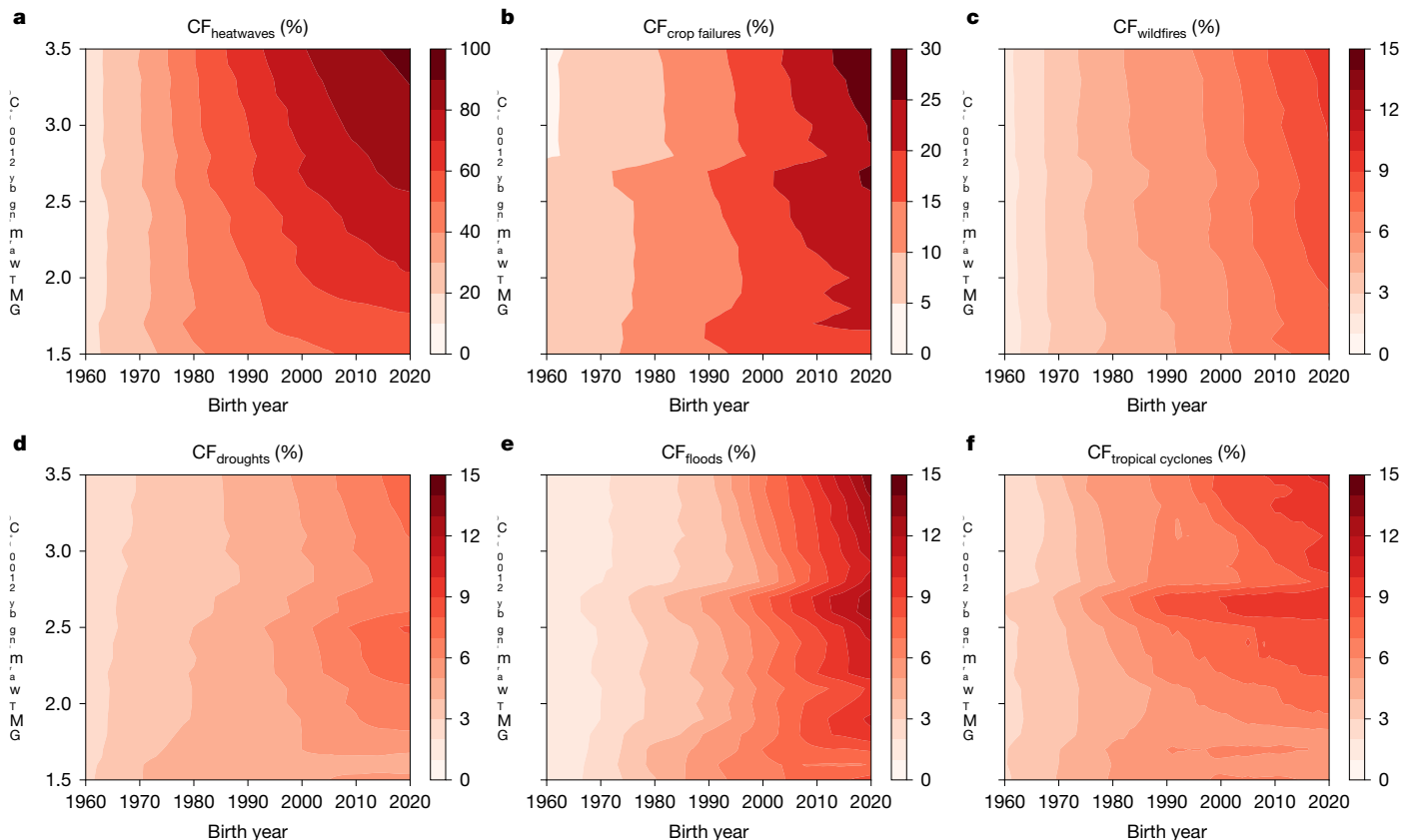


图3 | 在年轻一代和更高的变暖途径中，更大的前所未有的气候暴露。在所有出生年份（1960-2020）和GMT途径（1.5-3.5 °C）的A-D，队列分数（CF）（cf<sub>heatwaves</sub>; a），作物失败（cf<sub>crop failures</sub>; b），野火（cf<sub>heatwaves</sub>; a），野火（cf<sub>crop failures</sub>；c），河流洪水（CF<sub>floods</sub>；E）和热带气旋（CF<sub>tropical cyclones</sub>；F）。每个极端事件面板都有其颜色条范围。

小组面向热浪，而低剥夺组的78%（1900万）。当使用GDP时，这种差异是相似的，但是只有1974年和后来出生的年份在脆弱性层面上存在显著差异（补充图7）。在这里，在2020年出生年中，低收入组中有92%（2200万）在当前的政策下面对ULE，而高收入组为79%（1900万）。在1.5 °C和3.5 °C的替代变暖路径下，尽管相同的差异方向在脆弱性层面上保持相同的方向，但最低的脆弱性组（低剥夺和高GDP）受益于低温途径（图）。社会经济上脆弱的群体具有较低的自适应能力，并且在实施有效的适应措施<sup>18,19</sup>时面临更多限制。我们的结果强调了这些具有最高社会经济脆弱性和较低适应潜力的群体面临着前所未有的热波暴露的最高机会（图4）。根据过去和将来的极端气候，这强调了被剥夺社区的不成比例风险。

在全球范围内提供我们大部分热量摄入量的主要面包篮国家，迫使市场不稳定性只有最富有的人才能应对<sup>25</sup>。这些缺失的非本地影响使我们的估计是保守的。

相比之下，我们不会捕获人们如何适应极端，从而有可能减少其暴露或脆弱性。例如，可以减少有能力获得空调<sup>18</sup>的人群的接触。但是，对气候极端的玛拉（Mala）限制性反应可以创建脆弱性和暴露<sup>1</sup>的锁定。因此，我们的终生暴露估计忽略了有益的适应结果以及有害的非本地和不适当效应。最后，选择低于99.99%的阈值将降低标准杆并增加ULE估计，反之亦然。然而，这种效果受到限制，因为参考分布通常由小整数组成。相比之下，在自举数据样本（方法）中，使用高于99.99%的阈值冗余风险。

## 讨论

我们的分析仅通过设计来量化当地风险；然而，实际上，气候极端的效果是非局部级联的。例如，在2023年，来自加拿大活跃的野火季节的烟雾沿美国东海岸向南运输，使数百万人暴露于危险的空气质量<sup>20</sup>，并造成了增加的心脏疾病负担<sup>21</sup>。气候极端也通过经济影响影响社会，包括由于供应链中断<sup>22</sup>的生活成本的上升和征税，以恢复公共基础设施<sup>23</sup>。例如，气候变化在

这里没有考虑某些人口统计学现实。诸如国家内部迁移，生育能力和死亡率等因素实际上对这里考虑的极端<sup>11</sup>作出了反应。在美国，在这项研究中，人口面临所有极端的暴露，城市中心吸引了年轻人<sup>26</sup>和预期寿命的差异，在种族 - 县组合中都发现了<sup>27</sup>和农村 - 城市居住地<sup>28</sup>。例如，对于居住在城市的人来说，预期寿命更长，但是在这里，我们在每个国家/地区都统一地应用了国家平均的预期寿命和队列规模分布。此外，我们不考虑网格内部的异质性，也就是说，我们错过了社会经济脆弱性和社会经济多元化地区（例如城市）的一些细微规模的变化。最后，我们专注于脆弱性的社会经济层面，

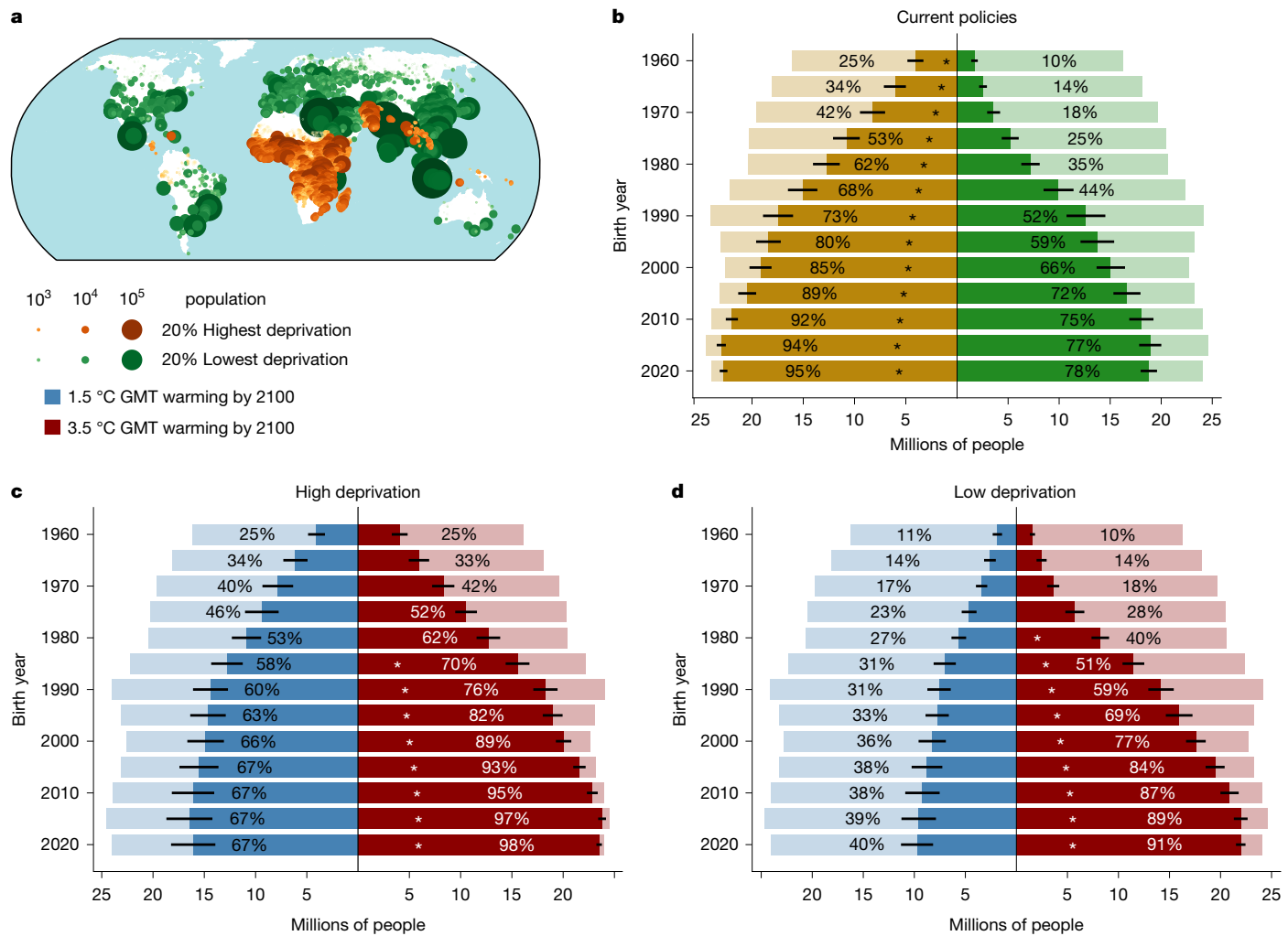


**Fig. 4 | The most deprived face significantly higher chance of ULE to heatwaves.** **a**, Geographic distribution of the 20% highest (brown markers) and 20% lowest (green markers) scoring 2020 birth cohort members (with roughly equal population) in the GRDI<sup>16</sup>. Grid cell marker sizes and colours are scaled by their population. **b**, Fraction of these two groups projected to experience ULE to heatwaves under the current policies pathway of 2.7 °C warming by 2100 for every fifth birth year. Light-coloured bars show total cohort sizes per birth year

and vulnerability group, whereas dark colours indicate the affected fraction. Error bars show the standard deviation across projections. Asterisks indicate that a low- or high-vulnerability group from a given birth cohort has significantly more members with ULE to heatwaves than the alternative vulnerability group of the same birth cohort (at the 5% level). **c,d**, The high deprivation (**c**) and low deprivation (**d**) share of the birth cohort that is projected to experience ULE under the 1.5 °C (blue) and 3.5 °C (red) pathways.

thereby neglecting that vulnerability to climate extremes may also vary with, for instance, age, gender or disability status. As demographic and multidimensional vulnerability information becomes available at ever higher spatial resolution and explicitly accounts for climate impact projections, it will become possible to deepen the analysis of the interaction between climate change and population dynamics.

The uncertainties of the extremes other than heatwaves are non-negligible. Hydrological variables have high internal climate variability<sup>29</sup> and projecting these events requires an additional impact-modelling step relative to heatwaves, which are computed directly from global climate model output (Methods). Furthermore, these events have sensitivities to input data quality and process representation across the modelling chain (Supplementary Note 2). Other uncertainties, such as demographic representation, are not captured in this analysis. Finally, we opt for assessing ULE at the grid scale instead of at the country level. In doing so, we downscale demographic data instead of upscaling climate data, thereby projecting lifetime exposure based on the local climate of individual birth cohort members. This incurs a trade-off for accepting natural variability in locations at

which ULE occurs, yet minimizing year-to-year variability in country- and global-scale CF estimates (Supplementary Note 3 and Supplementary Fig. 8).

## Conclusions

In summary, we find that large fractions of global birth cohorts are projected to live unprecedented exposure to heatwaves, river floods, droughts, crop failures, wildfires and tropical cyclones. As the frequency of these six climate extremes increases with warming, so does the fraction of people who will face ULE to these events. More ambitious policies are needed to achieve the goal of the Paris Agreement of limiting global warming to 1.5 °C by 2100 relative to the 2.7 °C warming expected under current policies, especially as the most vulnerable groups have more members projected to face unprecedented exposure to heatwaves. Children would reap the direct benefits of this increased ambition: a total of 613 million children born between 2003 and 2020 would then avoid ULE to heatwaves. For crop failures, this is 98 million, for river floods 64 million, for tropical cyclones 76 million, for droughts 26 million and for wildfires 17 million. This underlines the urgent need

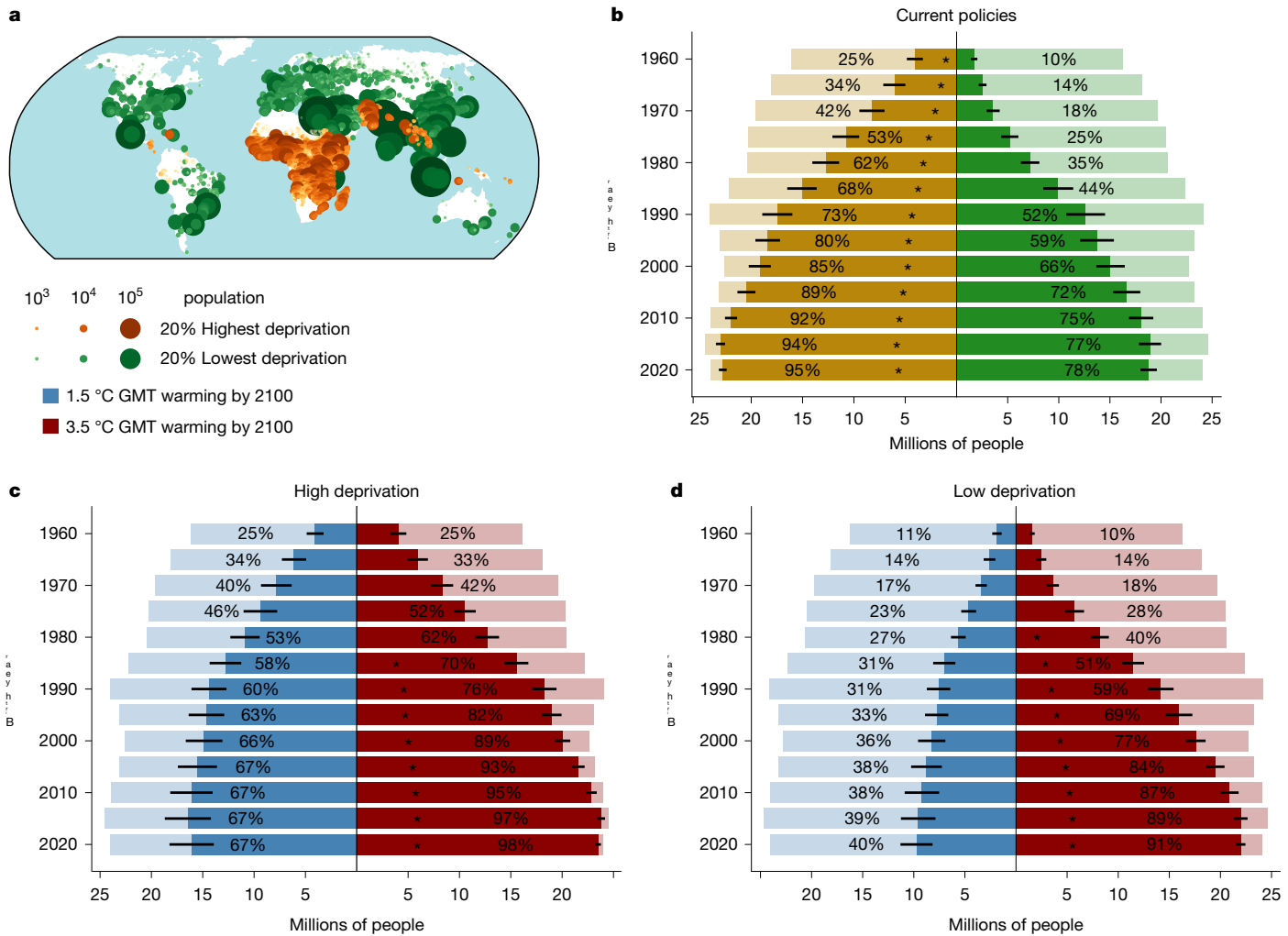


图4 | 最剥削的脸部ule的机会明显更高热浪。A，最高20%（棕色标记）的地理分布和在GRDI<sup>16</sup>中，2020年分娩队列成员（绿色标记）得分最低20%（绿色标记）。网格细胞标记的大小和颜色由其种群缩放。B，这两组预计在当前的政策途径2.7 °C的当前政策途径下，每五个出生年度将2100升温2100。浅色酒吧显示每个出生年的总体大小

和脆弱性组，而深色表示受影响的部分。错误条显示了跨预测的标准偏差。星号表明，来自给定的出生队列的低或高v弱者组的成员比相同出生队列的替代脆弱性组（在5%的水平上）要多得多。C，D，高剥削（C）和低剥削（D）的份额，预计将在1.5 °C (blue)和3.5 °C °C (RED {V16 RED})路径下经历ULE。

从而忽略了极端气候的脆弱性也可能随着年龄、性别或残疾状态而变化。随着较高的空间分辨率和明确说明气候影响预测的效率和多维脆弱性信息，可以加深对气候变化与人口动态之间相互作用的分析。

发生的情况是，但最小化国家和全球规模的CF估计值的年度变化（补充说明3和补充图。图。8）。

## 结论

总而言之，我们发现，全球出生队列的大量部分预计将实现前所未有的接触热水，河流洪水，干旱，农作物失败，野火和热带气旋。随着这六个极端气候的频率随着变暖的增长而增加，将面对这些事件的一部分也是如此。需要更多的政策来实现巴黎协议的目标，即相对于2.7 °C的2.7 °C的变暖，将全球变暖限制为1.5 °C 2100，尤其是因为最脆弱的群体预计，最易受伤害的群体预计有更多的成员受到预测前所未有的接触热门曝光。儿童将获得这一雄心勃勃的直接利益：2003年至2020年之间总共有6.13亿儿童将避免使用热浪。对于农作物的失败，这是9800万，对于河流洪水为6,400万，热带气旋7600万，干旱2600万，野火为1700万。这强调了迫切需要

for deep and sustained greenhouse gas emission reductions to safeguard the future of current young generations.

## Online content

Any methods, additional references, Nature Portfolio reporting summaries, source data, extended data, supplementary information, acknowledgements, peer review information; details of author contributions and competing interests; and statements of data and code availability are available at <https://doi.org/10.1038/s41586-025-08907-1>.

1. IPCC. *Climate Change 2022: Impacts, Adaptation and Vulnerability. Contribution of Working Group II to the Sixth Assessment Report of the Intergovernmental Panel on Climate Change* (Cambridge Univ. Press, 2022).
2. Burton, C. et al. Global burned area increasingly explained by climate change. *Nat. Clim. Change* **14**, 1186–1192 (2024).
3. Seneviratne, S. I. et al. in *Climate Change 2021: The Physical Science Basis. Contribution of Working Group I to the Sixth Assessment Report of the Intergovernmental Panel on Climate Change* (eds Masson-Delmotte, V. et al.) (Cambridge Univ. Press, 2021).
4. Cook, B. I. et al. Twenty-first century drought projections in the CMIP6 forcing scenarios. *Earth's Future* **8**, 2019–001461 (2020).
5. Domeisen, D. I. V. et al. Prediction and projection of heatwaves. *Nat. Rev. Earth Environ.* **4**, 36–50 (2023).
6. Gaupp, F., Hall, J., Mitchell, D. & Dadson, S. Increasing risks of multiple breadbasket failure under 1.5 and 2°C global warming. *Agric. Syst.* **175**, 34–45 (2019).
7. Yu, Y. et al. Machine learning-based observation-constrained projections reveal elevated global socioeconomic risks from wildfire. *Nat. Commun.* **13**, 1250 (2022).
8. Hirabayashi, Y. et al. Global flood risk under climate change. *Nat. Clim. Change* **3**, 816–821 (2013).
9. Knutson, T. R. et al. Tropical cyclones and climate change. *Nat. Geosci.* **3**, 157–163 (2010).
10. Climate Action Tracker. *The CAT Thermometer*. <https://climateactiontracker.org/global/cat-thermometer> (2022).
11. Thiery, W. et al. Intergenerational inequities in exposure to climate extremes. *Science* **374**, 158–160 (2021).
12. Lange, S. et al. Projecting exposure to extreme climate impact events across six event categories and three spatial scales. *Earth's Future* **8**, e2020EF001616 (2020).
13. Wan, H., Zhang, X., Zwiers, F. & Min, S.-K. Attributing northern high-latitude precipitation change over the period 1966–2005 to human influence. *Clim. Dyn.* **45**, 1713–1726 (2015).
14. Knutson, T. R. & Zeng, F. Model assessment of observed precipitation trends over land regions: detectable human influences and Possible low bias in model trends. *J. Clim.* **31**, 4617–4637 (2018).
15. Wang, Y. et al. Influence of anthropogenic and natural forcings on future changes in precipitation projected by the CMIP6-DAMIP models. *Int. J. Climatol.* **43**, 3892–3906 (2023).
16. Center for International Earth Science Information Network-CIESIN-Columbia University. *Global Gridded Relative Deprivation Index (GRDI), Version 1* (NASA Socioeconomic Data and Applications Center, 2022).
17. Frieler, K. et al. Assessing the impacts of 1.5°C global warming – simulation protocol of the Inter-Sectoral Impact Model Intercomparison Project (ISIMIP2b). *Geosci. Model Dev.* **10**, 4321–4345 (2017).
18. Andrijevic, M., Byers, E., Mastrucci, A., Smits, J. & Fuss, S. Future cooling gap in shared socioeconomic pathways. *Environ. Res. Lett.* **16**, 94053 (2021).
19. Andrijevic, M. et al. Towards scenario representation of adaptive capacity for global climate change assessments. *Nat. Clim. Change* **13**, 778–787 (2023).
20. Jain, P. et al. Drivers and impacts of the record-breaking 2023 wildfire season in Canada. *Nat. Commun.* **15**, 6764 (2024).
21. Maldarelli, M. E. et al. Polluted air from Canadian wildfires and cardiopulmonary disease in the Eastern US. *JAMA Netw. Open* **7**, 2450759–2450759 (2024).
22. Franzke, C. L. E. Impacts of a changing climate on economic damages and insurance. *Econ. Disasters Clim. Change* **1**, 95–110 (2017).
23. Cigler, B. A. U.S. floods: the necessity of mitigation. *State Local Gov. Rev.* **49**, 127–139 (2017).
24. Caparas, M., Zobel, Z., Castanho, A. D. A. & Schwalm, C. R. Increasing risks of crop failure and water scarcity in global breadbaskets by 2030. *Environ. Res. Lett.* **16**, 104013 (2021).
25. Tigchelaar, M., Battisti, D. S., Naylor, R. L. & Ray, D. K. Future warming increases probability of globally synchronized maize production shocks. *Proc. Natl. Acad. Sci. USA* **115**, 6644–6649 (2018).
26. Lee, Y., Lee, B. & Shubro, M. T. H. Urban revival by millennials? Intraurban net migration patterns of young adults, 1980–2010. *J. Reg. Sci.* **59**, 538–566 (2019).
27. Murray, C. J. L. et al. Eight Americas: investigating mortality disparities across races, counties, and race-counties in the United States. *PLoS Med.* **3**, 1513–1524 (2006).
28. Singh, G. K. & Siahpush, M. Widening rural–urban disparities in life expectancy, U.S., 1969–2009. *Am. J. Prev. Med.* **46**, e19–e29 (2014).
29. Douville, H. et al. in *Climate Change 2021: The Physical Science Basis. Contribution of Working Group I to the Sixth Assessment Report of the Intergovernmental Panel on Climate Change* (eds Masson-Delmotte, V. et al.) (Cambridge Univ. Press, 2021).

**Publisher's note** Springer Nature remains neutral with regard to jurisdictional claims in published maps and institutional affiliations.



**Open Access** This article is licensed under a Creative Commons Attribution 4.0 International License, which permits use, sharing, adaptation, distribution and reproduction in any medium or format, as long as you give appropriate credit to the original author(s) and the source, provide a link to the Creative Commons licence, and indicate if changes were made. The images or other third party material in this article are included in the article's Creative Commons licence, unless indicated otherwise in a credit line to the material. If material is not included in the article's Creative Commons licence and your intended use is not permitted by statutory regulation or exceeds the permitted use, you will need to obtain permission directly from the copyright holder. To view a copy of this licence, visit <http://creativecommons.org/licenses/by/4.0/>.

© Crown 2025

为了减少深层和持续的温室气体排放，以保护当前年轻一代的未来。

## 在线内容

任何方法，其他参考，自然投资组合报告概述，源数据，扩展数据，补充信息，确认，确认，同行审查信息；作者贡献和竞争利益的详细信息；数据和代码可用性的说明可在<https://doi.org/10.1038/s41586-025-08907-1>获得。

1. IPCC. *Climate Change 2022: Impacts, Adaptation and Vulnerability. Contribution of Working Group II to the Sixth Assessment Report of the Intergovernmental Panel on Climate Change* (Cambridge Univ. Press, 2022)。2. Burton, C. et al. 气候变化越来越多地解释了全球燃烧区域。 *Nat. Clim. Change* 14, 1186–1192 (2024)。3. Seneviratne, S. I. Et al. 在*Climate Change 2021: The Physical Science Basis. Contribution of Working Group I to the Sixth Assessment Report of the Intergovernmental Panel on Climate Change* (eds Masson-Delmotte, V. et al.) (Cambridge Univ. Press, 2021)。4. 库克, B. I. et al. CMIP6中的二十一世纪干旱预测迫使场景。 *Earth's Future* 8, 2019–001461 (2020)。5. Domeisen, D. I. V. et al. 热浪的预测和投影。 *Nat. Rev. Earth Environ.* 4, 36–50 (2023)。6. Gaupp, F., Hall, J., Mitchell, D. & Dadson, S. 在1.5和2 °C全球变暖下增加多个面包篮故障的风险。 *Agric. Syst.* 175, 34–45 (2019)。7. Yu, Y. et al. 基于机器学习的观察受限的预测显示，野火的全球社会经济风险升高。 *Nat. Commun.* 13, 1250 (2022)。8. Hira bayashi, Y. et al. 气候变化下的全球洪水风险。 *Nat. Clim. Change* 3, 816–821 (2013)。9. Knutson, T. R. Et al. 热带气旋和气候变化。 *Nat. Geosci.* 3, 157–163 (2010)。10. 气候动作跟踪器。 *The CAT Thermometer*. <https://climateactiontracker.org/global/cat-thermometer> (2022)。11. Thierry, W. et al. 暴露于气候极端的代际不平等。 *Science* 374, 158–160 (2021)。12. Lange, S. et al. 预测六个事件类别和三个空间量表的极端气候影响事件的暴露。 *Earth's Future* 8, E2020EF001616 (2020)。13. Wan, H., Zhang, X., Zwiers, F. & Min, S.-K. 将1966 - 2005年期间北部高纬度降水归因于人类影响力。 *Clim. Dyn.* 45, 1713–1726 (2015)。14. Knutson, T. R. & Zeng, F. 土地区域观察到的降水趋势的模型评估：可检测到的人类影响力和模型趋势中可能的低偏差。 *J. Clim.* 31, 4617–4637 (2018)。15. Wang, Y. et al. 人为和自然强迫对CMIP6-DAMIP模型预测的降水变化的影响。 *Int. J. Climatol.* 43, 3892–3906 (2023)。

16. 国际地球科学信息网络Ciesin-Columbia University. *Global Gridded Relative Deprivation Index (GRDI), Version 1* (NASA社会经济数据和应用中心, 2022年)。17. Frieler, K. et al. 评估1.5 °C全球变暖的影响 - 部门影响模型对比项目 (ISIMIP2B) 的仿真方案。 *Geosci. Model Dev.* 10, 4321–4345 (2017)。18. *Environ. Res. Lett.* 16, 940 53 (2021)。19. 倾向于代表全球气候变化评估的适应能力。 *Nat. Clim. Change* 13, 778–787 (2023)。20. Jain, P. et al. 加拿大2023年纪录的2023年野火季节破纪录的驾驶员和影响。 *Nat. Commun.* 15, 6764 (2024)。21. Maldarelli, M. E. et al. 美国东部的加拿大野火和心肺疾病受到污染的空气。 *JAMA Netw. Open* 7, 2450759–2450759 (2024)。22. Franzke, C. L. E. 气候变化对经济损失和保险的影响。 *Econ. Disasters Clim. Change* 1, 95–110 (2017)。23. State Local Gov. Rev. 49, 127–139 (2017)。24. Caparas, M., Zobel, Z., Castanho, A., D. A. & Schwalm, C. R. 到2030年，全球面包板中农作物衰竭和水稀缺的风险增加。 *Environ. Res. Lett.* 16, 104013 (2021)。25. Tigchelaar, M., Battisti, D. S., Naylor, R. L. & Ray, D. K. 未来变暖增加了全球同步玉米生产冲击的可能性。 *Proc. Natl. Acad. Sci. USA* 115, 6644–6649 (2018)。26. Lee, Y., Lee, B. & Shubrook, M. T. H. 千禧一代的Urban Revival？年轻人的郊区净迁移模式，1980 - 2010年。 *J. Reg. Sci.* 59, 538–566 (2019)。27. Murray, C. J. L. Et al. 八个美洲：调查种族，县的死亡率差异，

和美国的比赛。 *PLoS Med.* 3, 1513–1524 (2006)。28. Singh, G. K. & Siahpush, M. 预期寿命的农村 - 城市差异，1969–2009年。 *Am. J. Prev. Med.* 46, E19 – E29 (2014)。29. Douville, H. et al. 在*Climate Change 2021: The Physical Science Basis. Contribution of Working Group I to the Sixth Assessment Report of the Intergovernmental Panel on Climate Change* (Eds Masson-Delmotte, V. et al.) (Cambridge Univ. Press, 2021)。

出版商的注释Springer自然在已发表的地图和机构隶属关系中的管辖权主张方面仍然保持中立。



开放访问本文是根据创意共享归因4.0国际许可证的许可，该许可允许以任何媒介或格式使用，共享，适应，分发和复制，只要您提供适当的

归功于原始作者和来源，提供了与Creative Commons许可证的链接，并指出是否进行了更改。本文中的图像或其他第三方材料包含在文章的Creative Commons许可证中，除非在信用额度中另有说明。如果文章的创意共享许可中未包含材料，并且您的预期用途不得由法定法规允许或超过允许的用途，则需要直接从版权所有者那里获得许可。要查看此许可证的副本，请访问<http://creativecommons.org/licenses/4.0/>。

© Crown 2025

# Article

## Methods

### ISIMIP and exposure projections

The Inter-Sectoral Impact Model Intercomparison Project (ISIMIP) provides a simulation protocol for projecting the impacts of climate change across sectors such as biomes, agriculture, lakes, water, fisheries, marine ecosystems and permafrost ([www.isimip.org](http://www.isimip.org)). In ISIMIP2b, impact models representing these sectors are run using atmospheric boundary conditions from a consistent set of bias-adjusted global climate models (GCMs) from phase 5 of the Coupled Model Intercomparison Project (CMIP5) that were selected based on their availability of daily data and ability to represent a range of climate sensitivities<sup>17</sup>; the Geophysical Fluid Dynamics Laboratory Earth System Model (GFDL-ESM2M; ref. 30), the earth system configuration of the Hadley Centre Global Environmental Model (HadGEM2-ES; ref. 31), the general circulation model from the Institut Pierre-Simon Laplace Coupled Model (IPSL-CM5A-LR; ref. 32) and the Model for Interdisciplinary Research on Climate (MIROC5; ref. 33). Impact simulations are run for pre-industrial control (286 ppm CO<sub>2</sub>; 1666–2099), historical (1861–2005) and future (2006–2099) periods. Future simulations are based on Representative Concentration Pathways (RCPs) 2.6, 6.0 and 8.5 of GCM input datasets. Global projections of annual, grid-scale fractions of exposure to each extreme event category are calculated from ISIMIP2b impact simulations and GCM input data. For the full details of these computations, we refer to ref. 12, but we summarize extreme event definitions below.

For heatwaves, droughts, crop failures and river floods, we use localized pre-industrial thresholds to determine event occurrences, whereas for tropical cyclones, we use a single absolute threshold, and wildfires are modelled explicitly (Supplementary Table 20). Heatwaves affect an entire grid cell if the Heat Wave Magnitude Index daily (HWMid; refs. 34,35) of that year exceeds a threshold in the pre-industrial control HWMid distribution in that grid cell<sup>11</sup>. Although we refer to heatwaves throughout the paper, our definition technically refers to a 3-day extreme heat event that is expected on average once per century under pre-industrial climate conditions. These extreme heat events occur, by definition, everywhere across the world, but with different associated absolute temperature values. Previous analysis highlighted that intergenerational inequalities in lifetime heatwave exposure are robust across a range of heatwave definitions<sup>11</sup>. Crop failures are based on the sum of the area occupied by maize, wheat, soy or rice within a grid cell when their simulated yield falls below a threshold of their pre-industrial reference yield. Droughts, such as heatwaves, affect an entire grid cell if, for 7 months, monthly soil moisture remains below a threshold of pre-industrial soil moisture levels. Floods only correspond to river flooding, and the flooded area is derived from comparing daily discharge simulations from models of the global water sector to pre-industrial discharge. CaMa-Flood, a global river-routing model<sup>36</sup>, is used to convert these discharge values to flooded areas. Tropical cyclones occur if a grid cell sustains hurricane-force winds ( $\geq 64$  knots) at least once a year<sup>37,38</sup>. Exposure to tropical cyclones does not encompass the flood hazards typically associated with tropical cyclones. Wildfires occur when the burnt area is simulated in a grid cell. Burnt area is either taken directly from annual burnt area calculations or as the annual sum of monthly burnt area in cases in which impact models simulate burnt area sub-annually, capped at 100% of a grid cell. We reiterate that all exposure definitions here neglect potential exposure reduction measures and non-local effects.

We subsequently quantify human exposure to climate extremes in a way that facilitates comparison and aggregation across extreme event categories. We consider all people in a grid cell exposed to a climate extreme in a particular year if the climate extreme occurs in that year. We thereby assume that if such a river flood or wildfire occurs somewhere in a  $0.5^\circ \times 0.5^\circ$  grid cell, this is sufficiently close to any person located in that grid cell to be considered affected by this extreme

event. Using demographic data (see below), we subsequently convert this annual human exposure to lifetime exposure of birth cohorts by summing annual grid fractions of individual event categories across their lifetimes.

### Demographics

Demographic data for population totals, cohort sizes and life expectancy enable our projection of the CF experiencing ULE to these six extremes. Population totals at the grid scale come from the ISIMIP database (Fig. 2b; ref. 17) and originate from population estimates from v.3.2 of the History Database of the Global Environment (HYDE3.2; refs. 39,40) for the historical period (1860–2000) and population projections from middle-of-the-road Shared Socioeconomic Pathway (SSP2; refs. 41,42) for the future period (2010–2100). We note that these datasets at present do not account for the impact of climate on population dynamics, for example, through changes in migration, fertility and mortality, although these feedbacks may substantially alter the demographic data. Cohort sizes from the Wittgenstein Centre for Demography and Global Human Capital<sup>43</sup> provide estimates of country-level population totals every 5 years (between 1950 and 2100) for each 5-year age group (0- to 4-year-olds, 5- to 9-year-olds, and so on, until 95- to 99-year-olds and a final age group for those 100 years and older). Life expectancy data come from the United Nations World Population Prospects (UNWPP; ref. 44) and describe the life expectancy of 5-year-olds at the country level for 5-year blocks (1950–1955 to 2015–2020). In this dataset, life expectancy is reported for 5-year-olds to exclude biases from infant mortality. Countries that can be spatially resolved at the ISIMIP grid scale and have cohort and life expectancy estimates in these datasets meet the requirements of this study and total 177. We refer to the supplementary material of ref. 11 for a broader discussion of these datasets but explain our application of them in this analysis below.

All demographic datasets are modified to represent lifetimes annually, beginning from 1960 to 2020. Life expectancies for each country are first linearly interpolated to annual values by assuming that the values of the original 5-year groups are representative of the middle of that group. Furthermore, we add 5 years to annual life expectancies to capture the life expectancy of each cohort since birth, as the original data begin at age 5. As the maximum UNWPP life expectancy for people born in 2020 prescribes the final year in this analysis (2113), annual population totals must be extrapolated to reach this year. For population totals, we take each year beyond 2100 as the mean of the preceding 10 years of the dataset, such that population numbers for 2101 are the mean of 2091–2100. For cohort sizes in each country, we interpolate annual cohort sizes and age groups from the original 5-year age groups and divide age totals by 5 to maintain original population sizes in this dataset and linearly extrapolate these estimates to 2113. This provides the absolute numbers of 0- to 100-year-olds for each year across 1960–2113.

To downscale this demographic information to the grid scale, we assume spatially homogeneous cohort representation and life expectancy. Birth cohort size is represented as the number of people of age 0 of a given birth year in a given grid cell. This is estimated by multiplying the absolute population of the birth year (using the annual grid-scale population totals from ISIMIP) by the relative size of the age 0 cohort (using the interpolated 0- to 100-year-old population totals from the Wittgenstein Centre cohort data). Spatial variability in age structure and life expectancy within a country is therefore ignored in this study.

### Mapping impacts to GMT trajectories

To project CF across different warming pathways by 2100, we construct a series of incrementally warming GMT pathways between 1960 and 2113 based on GMT trajectories taken from the AR6 Scenario Explorer<sup>45</sup>. The time series from the AR6 scenario explorer were chosen as anchor points for interpolation to produce a range of plausible GMT time series. Furthermore, they were selected to minimize overshooting in the early

# 文章

## 方法

### Isimip和曝光预测

部门间影响模型比较项目 (ISIMIP) 提供了一种模拟协议，用于投影跨生物群落，农业，湖泊，水，渔业，海洋生态系统和永久弗罗斯特等部门的气候变化的影响 ([www.isimip.org](http://www.isimip.org))。在ISIMIP2B中，代表这些部门的影响模型是使用震荡边界条件运行的，该条件是从一致的偏置调整后的全球气候模型 (GCMS (GCM)) (GCMS) 中，偶联模型对间隔项目 (CMIP5) 的5阶段 (CMIP5) 根据每日数据的可用性和代表气候敏感性的范围的范围而被选择的能力来选择的，这些模型; system模型 (gfdl-esm2m; ref. 30)，哈德利中心全球环境模型 (hadgem2-es; ref. 31) 的地球系统配置，31)，，，来自Institut pierre-simon lapaplace c oupl coupl coupled coupl cou ipl cou iple cou iple cou iple counter 参考 32) 和气候间纪律研究模型 (Miroc5; ref. 33)。对工业前控制 (286 P PM CO<sub>2</sub>; 1666–2099)，历史 (1861–2005) 和Future (Future (2006–2099) 时期运行影响模拟。未来的模拟基于GCM输入数据集的代表性浓度途径 (RCP) 2.6、6.0和8.5。从ISIMIP2B影响模拟和GCM输入数据计算的每个极端事件类别的年度，网格尺度差异的全球预测。有关这些计算的全部详细信息，我们参考参考文献 12，但我们总结了下面的极端事件定义。

对于热浪，干旱，农作物故障和河流洪水，我们使用本地工业前阈值来确定事件发生，而对于热带旋风，我们使用单个绝对阈值，并明确地对野火进行建模 (补充表 20)。如果热浪幅度指数每天 (HWMID; 参考文献。尽管我们在整个论文中指的是热浪，但我们的定义在技术上是指在工业前气候条件下平均每一世纪一次的3天极端热事件。从定义上讲，这些极端热量事件发生在世界各地，但具有不同相关的绝对温度值。先前的分析表明，在一系列热浪定义<sup>11</sup>中，寿命热波暴露的代际不平等是可靠的。农作物失败是基于玉米，小麦，大豆或大米在网格电池内占据的面积的总和，当它们的模拟产量低于其工业前参考产率的阈值。如果在7个月内，每月的土壤水分保持低于工业前土壤水分水平的阈值，则干旱 (例如热浪) 会影响整个网格电池。洪水仅构成河流洪水，而洪水泛滥的区域源于比较全球水部门模型与工业前出院的每日排放模拟。Cama-Flood是一种全球河道模型<sup>36</sup>，用于将这些排放值转换为被洪水淹没的地区。如果网格电池维持飓风风 ( $\geq 64$  节)，则会发生热带气旋。暴露于热带气旋不会通过通常与热带气旋相关的洪水危害。当在网格电池中模拟燃烧区域时，就会发生野火。烧伤面积直接取自年度烧毁面积的计算，也可以作为每月烧毁面积的总和，而影响模型则在次生上模拟烧毁的区域，限制为100%的网格电池。我们重申，这里的所有暴露定义都忽略了潜在的降低暴露措施和非本地影响。

随后，我们以促进极端事件类别的比较和聚集的方式量化了人类对气候极端的暴露。如果气候极端发生在那一年，我们考虑在特定年内暴露于气候极端的网格电池中的所有人。因此，我们假设，如果这种河流洪水或野火发生在 $0.5^\circ \times 0.5^\circ$ 网格电池中，则足够接近该网格电池中的任何person子，都被认为受到这种极端的影响

事件。使用人口统计数据 (请参阅下文)，我们随后将这种年度人类的暴露转换为终生暴露于出生队列的终生暴露，通过将各个事件类别的年度栅格分数在其一生中求和。

### 人口统计

人口数据的人口数据总数，人群规模和寿命指出，我们可以投射出这六个极端的CF。网格量表的人口来自ISIMIP数据库 (图 2b; 参考 17)，源自来自全球环境历史数据库的v.3.2的人口估计 (hyde3.2; refs)。未来期间 (2010–2100) 的途径 (SSP2; 参考 41,42)。我们注意到，这些数据集目前尚未解释气候对人口动态的影响，例如，通过迁移，生育和死亡率的变化，尽管这些反馈可能会大大改变示例数据。Vittgenstein De maphy和全球人力资本中心的同类尺寸<sup>43</sup>估计每5年年龄段 (1950年至2100年之间)，每5年年龄段 (1950年至2100年之间) (0至4岁至4岁至4岁，5至9岁的孩子)，直到95至99岁和99岁的年龄段和V2年龄的年龄为100岁)。预期寿命数据来自联合国世界人口职业 (UNDPP; 参考 44)，并描述了5年街区 (1950–1955至2015 – 2020年) 在该国级别的5岁儿童的预期寿命。在此数据集中，据报道5岁儿童将寿命排除在婴儿死亡率之外。可以在ISIMIP网格量表上在空间上解决的国家，并且在这些数据集中具有队列和预期寿命估计值满足这项研究的要求，总计177。我们指的是参考文献 11的补充材料，以对这些数据集进行更广泛的讨论，但在下面的分析中对他们的应用进行了更广泛的讨论。

从1960年到2020年，所有人口数据集都经过修改以表示寿命。每个国家的预期终身是通过假设原始5年组的价值代表该组中间的，首先是线性插值到年度价值的。此外，我们期望每年的寿命增加5 年，以捕获自出生以来每个人群的预期寿命，因为原始数据始于5岁。由于2020年出生的人的最高预期寿命是在本分析中的最后一年 (2113) 规定 (2113)，年度人口的总数必须超过本年度。对于人口的总数，我们每年将2100以上的时间作为数据集的前10个年的平均值，因此2101的人口数量是2091 – 2100年的平均值。对于每个国家的队列大小，我们插入了来自原始5岁年龄段的年度群体大小和年龄段，并将年龄总数除以5年，以维持该数据集中的原始人口规模，并将这些估计值线性推送到2113。这提供了整个1960 – 2113年每年的绝对数量为0–2113。

为了将这些人口统计信息降低到网格量表，我们假设在空间均匀的队列代表和生命期间。出生队列的大小表示为给定的网格单元中给定出生年的0岁人数。通过将出生年度的绝对人群 (使用Isimip的年度网格级人口总数) 乘以年龄为0年龄段 (使用Wittgenstein Center Center cohort数据的插值0至100年人口总数) 来估计。因此，本研究中忽略了一个国家的年龄结构和预期寿命的空间变化。

### 对GMT轨迹的映射影响

为了在2100年之前跨不同的变暖途径进行投影，我们根据从AR6场景Explorer<sup>45</sup>获得的GMT轨迹之间构建了一系列1960年至2113年之间的增量加热GMT途径。从AR6场景资源管理器中的时间序列被选为插值的锚点，以产生一系列合理的GMT时间序列。此外，他们被选中以最大程度地减少早期的过度旋

years of low GMT pathways over higher GMT pathways, which can skew lifetime exposure estimates for early birth cohorts (Supplementary Fig. 9). The upper bound of this subset was limited to 3.5 °C in favour of sampling more simulations for higher GMT projections, which we discuss further below. For the lower bound, 1.5 °C was chosen because it is a more realistic minimal warming scenario than 1.0 °C. Note that the 1.5 °C anchor scenario maximally reaches 1.57 °C before reducing to 1.5 °C by 2100. It is, therefore, referred to as 1.5 °C throughout this analysis. These warming levels are reported relative to pre-industrial temperatures from 1850 to 1900. This yields a total of 21 GMT pathways for which we project CF.

Our dataset of extreme event exposures represents occurrences of these extremes forced by GCM-modelled climates. These climates have unique GMT warming pathways that depend on their radiative forcing scenario (historical or RCP), as prescribed by the ISIMIP2b modelling protocol. To project these exposure maps along even intervals of warming scenarios, which the original simulations do not provide, we use the 21 GMT pathways described above. For each pairing of the 21 target GMT pathways and the concatenated historical and future exposure projections, we sample exposures by matching the GMT warming levels of the exposure series to the years of the target GMT pathways (Supplementary Figs. 9 and 10). The GMT warming levels behind the exposure projections are first smoothed with a 21-year rolling mean before GMT mapping is undertaken. In cases in which our constructed GMT pathways exceed the GMT warming levels of GCM simulations by too much, this mapping erroneously resamples the year of exposures corresponding to the maximum warming level of their forcing GCM. To this end, we implement a constraint in this sampling procedure such that GMT-mapped series are only used if the maximum difference across all GMT pairs is no larger than 0.2 °C. This constraint incrementally reduces ensemble sizes of exposure projections for higher GMT pathways (Supplementary Table 19).

### Lifetime exposure

Estimating lifetime exposure to extreme events requires crossing life expectancy data at the country level with grid-scale exposure projections. For each GMT trajectory (1.5–3.5 °C, 0.1 °C intervals), birth year (1960–2020) and country (177), exposures are summed across lifetimes at the grid scale. This assumes life expectancy to be spatially homogeneous across each country. Exposure during the death years is also included in this sum by multiplying these exposure projections by the fraction of the final year lived. This produces country-wide maps of lifetime exposure at the grid scale for each GMT trajectory and birth year in this analysis.

To generate a baseline distribution of lifetime exposure in a world without climate change, large samples of pre-industrial lifetime exposures are bootstrapped assuming 1960 life expectancy in each country. Here, for each exposure projection originating from a simulation under a pre-industrial climate, 10,000 lifetime exposures are estimated by resampling exposure years with replacement. Depending on ISIMIP2b data availability, pre-industrial exposure projections have a length of 239–639 years per simulation from which to resample from<sup>11</sup>. This process generates 40,000–310,000 country-wide maps of lifetime exposure, depending on the extreme event considered and its underlying data availability, enabling exposure projections in a pre-industrial climate. Using the pre-industrial period as a baseline enables (1) our GMT mapping procedure; (2) bootstrapping a stationary time series to achieve a large reference dataset; and (3) the production of a reference dataset with information that is independent of the projections forming our ULE estimates.

### Emergence of ULE

We define an emergence threshold for ULE to extreme events as the 99.99th percentile of our grid-scale samples of pre-industrial lifetime exposure. When it comes to the selection of this percentile, we went

as extreme as possible given the bootstrapping of the pre-industrial control runs. This choice was based on a sensitivity analysis for different percentile values that showed a levelling off of lifetime exposure for percentiles more extreme than 99.99%. This indicated that the 99.99th percentile achieves the limit of reliable information that can be extracted from the empirical distribution. For each extreme event, birth year, GMT pathway and grid cell, we assess if lifetime exposure emerges or passes this threshold of extreme exposure in a pre-industrial climate. If this threshold is passed, we consider the whole birth cohort in this grid cell to have emerged, tallying its size among a global pool of the same birth cohort and GMT trajectory of people projected to live ULE. This means that, in some locations, even if the sum of exposed grid cell fractions across a pre-industrial lifetime does not cover the entire grid cell, we still extract the entire birth cohort size associated with that grid cell. We sum the number of emerged people in each birth cohort globally, although this birth cohort has a different life expectancy in each country. Once the number of people who have emerged globally is tallied, we divide this by the respective total cohort sizes to estimate CF per birth cohort. Note that ULE, therefore, does not refer to unprecedented in terms of the magnitude of assets or people exposed, but rather in terms of the number of events accumulated across an average person's lifespan in comparison with what they would face in a pre-industrial climate.

### ULE across socioeconomic vulnerability strata

We use two grid-scale indicators of vulnerability to compare with our estimates of ULE to heat waves. The first is an ISIMIP2b GDP input dataset using concatenated historical and SSP2 time series covering 1860–2099 annually<sup>17</sup>. This dataset was disaggregated from the country to grid level using spatial and socioeconomic interactions among cities, land cover and road network information and SSP-prescribed estimates of rural and urban expansion<sup>46</sup>. The second indicator is the Global Gridded Relative Deprivation Index v.1 (GRDI; ref. 16), which communicates relative levels of multidimensional deprivation and poverty (0–100, least to most deprived). This deprivation score uses six input components. First is the child dependency ratio, which is the ratio between the population of children and the working-age population (15–64 years). This can indicate vulnerability, for which high ratios indicate a dependency of supposed consumers and non-producers on the working-age (producing) population<sup>47</sup>. Second, infant mortality rates (IMR), taken as the deaths in children younger than 1 year of age per 1,000 live births annually, are a signal of population health and form a long-term Sustainable Development Goal of the United Nations<sup>48</sup>. Third, the Subnational Human Development Index (SHDI), an assessment of human well-being across education, health and standard of living, originates from the Human Development Index, the latter of which is considered one of the most popular indices to assess country-level well-being. The SHDI improves on the HDI in terms of spatial scale and in representing 161 countries across all world regions and development levels<sup>49</sup>. Fourth, as rural populations are generally prone to multidimensional poverty<sup>50</sup>, low values in the ratio of built-up to non-built-up area (BUILT) signal high deprivation. The fifth and sixth components use the mean (of 2020; VNL 2020) and slope (2012–2020; VNL Slope) of nighttime light intensity, a proxy for human activity, economic output and infrastructure development<sup>51</sup>, to indicate deprivation for areas of low nighttime light intensity. These input components range from 30 arc seconds (roughly 1 km) resolution to subnational regions and are harmonized in an ArcGIS Fishnet feature class for aggregation onto a 0–100 range representing low to high deprivation. For the final aggregation, the IMR and SHDI components are given half the weight of the rest of the inputs, given their coarser resolution. The GRDI, therefore, encapsulates multiple dimensions through which generations face deprivation and therewith socioeconomic vulnerability to climate extremes. Although our approach does not explicitly account for actual or potential adaptation to climate change, this multidimensional approach to

GMT途径高的GMT途径的多年，这可能会使早期出生队列的寿命估计偏斜（补充图9）。该子集的上限限制为 $3.5^{\circ}\text{C}$ ，有利于对更高的GMT投影进行更多模拟，我们在下面进一步讨论。对于下限，选择了 $1.5^{\circ}\text{C}$ ，因为它比 $1.0^{\circ}\text{C}$ 更现实的最小变暖方案。请注意， $1.5^{\circ}\text{C}$ 锚点方案最大地达到 $1.57^{\circ}\text{C}$ ，然后将2100降低至 $1.5^{\circ}\text{C}$ 。因此，在整个分析过程中，它被称为 $1.5^{\circ}\text{C}$ 。据报道，这些变暖水平相对于从1850年到1900年的工业前温度。这总共产生了21 GMT途径，我们为此提出了cf。

我们的极端事件暴露数据集代表了GCM模型气候强迫的这些极端的发生。这些气候具有独特的GMT变暖途径，取决于ISIMIP2B Modelling协议规定的辐射强迫场景（历史或RCP）。为了将这些曝光图沿着温暖场景的间隔投影，原始模拟所没有提供的，我们使用上述21 GMT途径。对于21个目标GMT途径的每对配对以及串联的历史和未来的暴露预测，我们通过将暴露序列的GMT变暖水平与目标GMT途径的年份相匹配（补充图9和10）来取样暴露。在进行GMT映射之前，首先要平均使用21年的卷积，而在进行GMT的滚动下，GMT变暖水平首先要平滑。如果我们构造的GMT途径超过GCM模拟的GMT变暖水平过多，则该映射错误地重塑了与强迫GCM最大变暖水平相对应的暴露年份。为此，我们在此采样过程中实现了一个约束，因此仅当所有GMT对的最大差异不大于 $0.2^{\circ}\text{C}$ 时，才使用GMT映射序列。该约束逐渐减少了较高GMT途径的曝光投影的集合大小（补充表19）。

### 终身暴露

估计对极端事件的终生暴露需要通过网格尺度的暴露进程来跨越该国级别的预期寿命数据。对于每个GMT轨迹（ $1.5\text{--}3.5^{\circ}\text{C}$ ,  $0.1^{\circ}\text{C}$ 间隔），出生年份（1960-2020）和国家（177）（177），在网格量表上跨越了一生。这假定每个国家的预期寿命在空间上是均匀的。在死亡年份的暴露还包括将这些暴露预测乘以最后一年的寿命，包括这些款项。在此分析中，这会在每个GMT轨迹和出生年度的网格量表上生成全国范围内的终生暴露地图。

为了在没有气候变化的世界中产生终身暴露的基线分布，假设每个国家/地区的预期寿命为1960年的预期寿命，则在没有气候变化的情况下进行了大量样本。在这里，对于源自工业前气候下的模拟的每个暴露投影，通过替代品重新采样年度来估算10,000次终身暴露。根据ISIMIP2B数据的可用性，工业前的暴露预测的长度为239-639年，每个模拟从<sup>11</sup>重新样本。此过程可产生40,000-310,000个全国范围内的终生曝光地图，具体取决于所考虑的极端事件及其潜在的数据可用性，从而在工业前的气候下实现了暴露预测。使用前工业期作为基线启用（1）我们的GMT映射程序；（2）引导一个固定时间序列以获得大型参考数据集；（3）产生参考数据集，其中包含与构成ULE估计的预测的信息。

### Ule的出现

我们将ULE到极端事件的出现阈值定义为我们在工业前寿命暴露的网格尺度样本的第99.99个百分位数。当涉及到这个百分位的选择时，我们去了

鉴于前工业控制的自举，尽可能极端地运行。此选择是基于对不同百分位数值的敏感性分析，该分析表明，比99.99%的百分位数的终生暴露均升级。这表明第99.99个百分位数达到了可以从经验分布中提取的可靠信息的限制。对于每个极端事件，出生年份，GMT途径和网格电池，我们评估终生暴露是在工业前气候下出现还是通过这种极端暴露的阈值。如果通过这个阈值，我们认为该网格单元中的整个出生队列都出现了，将其大小统计在同一出生队列的全球池中，以及预计将居住ULE的人的GMT轨迹。这意味着，在某些位置，即使跨工业前寿命的暴露网格细胞分数的总和不涵盖整个网格单元，我们仍然提取与该网格单元相关的整个出生队列大小。我们将每个出生队列中每个出生队列中出现的人数总计，尽管这个出生队列在每个国家都有不同的生活。一旦掌握了全球出现的人数，我们就将其除以相应的总体大小以估算每个出生队列的CF。请注意，因此，ule并不是指空前的资产或暴露的人的大小，而是指与他们在前工业前气候中所面临的事件相比，在普通人的寿命中积累的事件数量。

### 整个社会经济脆弱性阶层

我们使用两个网格尺度脆弱性指标与我们对ULE的估计与热浪相比。第一个是使用串联的历史和SSP2时间序列覆盖1860-2099的ISIMIP2B GDP输入数据集。该数据集通过城市，土地覆盖和道路网络信息之间的空间和社会经济相互作用以及对农村和城市扩张的SSP规定估计<sup>46</sup>之间的空间和社会经济相互作用进行了分类。第二个指标是全局网格相对剥夺指数v.1（grdi; ref. 16），它传达了多维剥夺和贫困的相对水平（0-100，至少与大多数被剥夺）。这种剥夺分数使用六个输入组成。首先是儿童依赖比率，它是儿童人口与工作年龄人口（15-64年）之间的比率。这可能表明脆弱性，因为高比例表明所假定的消费者和非生产者对工作年龄（生产）人群<sup>47</sup>的依赖。其次，婴儿死亡率（IMR）是每年1000名活生生年龄少于1的儿童的死亡，这是人口健康的信号，并构成了联合国长期可维持的发展目标<sup>48</sup>。第三，跨教育，健康和生活水平的人类福祉的评估是人类发展指数，源自人类发展指数，后者被认为是评估国家水平福祉的最受欢迎指数之一。SHDI从空间量表和代表所有世界地区和发展水平的161个国家<sup>49</sup>方面改善了HDI。第四，由于农村人口通常容易出现多维贫困<sup>50</sup>，因此构建与非建造区域（已建造）信号高剥夺的比率低。第五和第六个组件使用平均值（2020；VNL 2020）和斜坡（2012-2020；VNL斜率）的夜间光强度，替代人类活动，经济产量和基础性发展<sup>51</sup>，以指示低夜间光强度区域的剥夺。这些输入组件的范围从30弧秒（大约1 km）分辨率到下部区域，并在ArcGIS渔网特征类中进行协调，用于聚集到代表低剥夺至高剥夺的0-100范围。对于最终聚合，鉴于其更粗的分辨率，IMR和SHDI组件的重量是其余输入的一半。因此，Grdi封装了多个维度，几代人面临剥夺，从而使社会经济脆弱性易受极端气候的脆弱性。尽管我们的方法并未明确说明对气候变化的实际或强大的适应性，但这种多维方法

# Article

vulnerability provides relevant information on the current adaptation potential of local populations.

We preprocess GDP and GRDI products to enable their comparison with our ULE estimates across birth years. For GDP, similar to other datasets in our analysis, we extend the series to 2113 to accommodate the longest life expectancy of the 2020 birth cohort by copying the final year of the original dataset. We then use our ISIMIP population totals to compute GDP per capita at the grid scale. Using the GDP per capita metric, we calculate lifetime mean GDP per capita using our life expectancy information for the 1960–2020 birth cohorts. We refer to lifetime mean GDP per capita as simply GDP. For GRDI, we conservatively regrid the original grid cells of about 1 km to the 0.5° ISIMIP grid. Although GRDI is a map composed of data spanning 2010–2020, we assume this to be representative of 2020, but nonetheless compare it with the 1960–2020 birth cohort range, similar to the rest of the analysis.

We then identify 20% quantile ranges (that is, (0–20], (20–40], ..., (80–100]) for the lifetime GDP of each birth year and for the singular GRDI map (assumed to align with 2020 population totals). To this end, we rank the vulnerability indicators and apply these ranks to our birth cohort totals on the same grid and for the matching year. For example, the ranks taken from the lifetime mean GDP of the 2020 birth cohort are aligned with the population totals of newborns in 2020. Finally, we bin the ranked vulnerability indicators by their associated population totals into five groups of nearly equal population (as it is not possible to achieve perfect bin sizes given the sums of grid-scale population totals). This groups the richest and poorest and least and most deprived into the aforementioned quantile ranges. The quantile range of each vulnerability indicator is then a map that can be used to mask the existing locations of ULE, such as birth years and all GMT pathways. With GRDI (Supplementary Fig. 11) and GDP (Supplementary Fig. 12), we compare the lowest and the highest 20% of each indicator by population.

## Data availability

The data for this analysis originate from multiple sources and are hereby listed. Model inputs, raw impact model simulations and post-processed extremes (the latter as Derived Output Data) from ISIMIP2b, as well as GDP data, are accessible at the ISIMIP repository here (<https://data.isimip.org>). Cohort sizes are taken from the Wittgenstein Centre for Demography and Global Human Capital (<https://dataexplorer.wittgensteincentre.org/wcde-v2>). Life expectancy data come from the UN demographics data portal (<https://population.un.org/dataportal/home?df=10750103-f8fa-4a7e-bb6a-b0f151970005>). Global mean temperatures are extracted from the AR6 scenario explorer<sup>45</sup> (<https://doi.org/10.5281/zenodo.7197970>). GRDI is hosted on the NASA EARTHDATA platform (<https://doi.org/10.7927/3xxe-ap97>). Maps in this analysis contain base map information made with Natural Earth ([naturalearth-data.com](http://naturalearth-data.com)).

## Code availability

The code for this analysis can be found at GitHub ([https://github.com/VUB-HYDR/2025\\_Grant\\_etal\\_Nature/tree/main](https://github.com/VUB-HYDR/2025_Grant_etal_Nature/tree/main)).

30. Dunne, J. P. et al. GFDL's ESM2 global coupled climate-carbon Earth system models. Part I: physical formulation and baseline simulation characteristics. *J. Clim.* **25**, 6646–6665 (2012).

31. Jones, C. D. et al. The HadGEM2-ES implementation of CMIP5 centennial simulations. *Geosci. Model Dev.* **4**, 543–570 (2011).
32. Dufresne, J.-L. et al. Climate change projections using the IPSL-CM5 Earth System Model: from CMIP3 to CMIP5. *Clim. Dyn.* **40**, 2123–2165 (2013).
33. Watanabe, M. et al. Improved climate simulation by MIROC5: mean states, variability, and climate sensitivity. *J. Clim.* **23**, 6312–6335 (2010).
34. Russo, S., Sillmann, J. & Fischer, E. M. Top ten European heatwaves since 1950 and their occurrence in the coming decades. *Environ. Res. Lett.* **10**, 124003 (2015).
35. Russo, S., Sillmann, J. & Sterl, A. Humid heat waves at different warming levels. *Sci. Rep.* **7**, 7477 (2017).
36. Yamazaki, D., Kanae, S., Kim, H. & Oki, T. A physically based description of floodplain inundation dynamics in a global river routing model. *Water Resour. Res.* **47**, W04501 (2011).
37. Emanuel, K. Downscaling CMIP5 climate models shows increased tropical cyclone activity over the 21st century. *Proc. Natl Acad. Sci. USA* **110**, 12219–12224 (2013).
38. Holland, G. A revised hurricane pressure-wind model. *Mon. Weather Rev.* **136**, 3432–3445 (2008).
39. Klein Goldewijk, K., Beusen, A. & Janssen, P. Long-term dynamic modeling of global population and built-up area in a spatially explicit way: HYDE 3.1. *Holocene* **20**, 565–573 (2010).
40. Klein Goldewijk, K., Beusen, A. & Drecht, G. V. The HYDE 3.1 spatially explicit database of human-induced global land-use change over the past 12,000 years. *Global Ecol. Biogeogr.* **20**, 73–86 (2011).
41. Fricko, O. et al. The marker quantification of the Shared Socioeconomic Pathway 2: a middle-of-the-road scenario for the 21st century. *Global Environ. Change* **42**, 251–267 (2017).
42. Samir, K. C. & Lutz, W. The human core of the shared socioeconomic pathways: population scenarios by age, sex and level of education for all countries to 2100. *Global Environ. Change* **42**, 181–192 (2017).
43. Lutz, W., Goujon, A., Samir, K. C., Stonawski, M. & Stilianakis, N. (eds) *Demographic and Human Capital Scenarios for the 21st Century: 2018 Assessment for 201 Countries* (Publications Office of the European Union, 2018).
44. United Nations Department of Economic and Social Affairs. *World Population Prospects 2019* (United Nations, 2019).
45. Byers, E. et al. AR6 Scenarios Database v1.1. Zenodo <https://doi.org/10.5281/zenodo.7197970> (2022).
46. Murakami, D. & Yamagata, Y. Estimation of gridded population and GDP scenarios with spatially explicit statistical downscaling. *Sustainability* **11**, 2106 (2019).
47. Bartram, L. & Roe, B. Dependency ratios: useful policy-making tools? *Geriatr. Gerontol. Int.* **5**, 224–228 (2005).
48. Sharroff, D. et al. Global, regional, and national trends in under-5 mortality between 1990 and 2019 with scenario-based projections until 2030: a systematic analysis by the UN Inter-agency Group for Child Mortality Estimation. *Lancet Glob. Health* **10**, 195–206 (2022).
49. Smits, J. & Permanyer, I. The Subnational Human Development Database. *Sci. Data* **6**, 190038 (2019).
50. Laborde Debucquet, D. & Martin, W. Implications of the global growth slowdown for rural poverty. *Agric. Econ.* **49**, 325–338 (2018).
51. Bruederle, A. & Hodler, R. Nighttime lights as a proxy for human development at the local level. *PLoS One* **13**, e0202231 (2018).

**Acknowledgements** We acknowledge the Potsdam Institute for Climate Impact Research (PIK) for their coordination of ISIMIP and the modellers contributing runs to ISIMIP2b. We thank M. Andrijevic, C.-F. Schleussner and E. Byers for their discussions regarding this paper. W.T. acknowledges funding from the European Research Council (ERC) under the Horizon Framework research and innovation programme of the European Union (grant agreement no. 101076909; ERC Consolidator Grant LACRIMA). We acknowledge further funding from the European Union under the grant agreement no. 101081369 (SPARCCLIE). The computational resources and services used in this work were provided by the VSC (Flemish Supercomputer Center), funded by the Research Foundation – Flanders (FWO) and the Flemish Government, department EWI. This work was supported by the Wellcome Trust 309498/Z/24/Z.

**Author contributions** L. Grant helped to conceive this study, performed the analysis and wrote the paper. W.T. helped to conceive the study and write the paper. I.V. helped with coding parts of this analysis and writing the paper. L. Gudmundsson, E.F. and S.I.S. helped generate ideas for the analysis and curate the paper.

**Competing interests** The authors declare no competing interests.

## Additional information

**Supplementary information** The online version contains supplementary material available at <https://doi.org/10.1038/s41586-025-08907-1>.

**Correspondence and requests for materials** should be addressed to Luke Grant.

**Peer review information** *Nature* thanks Stephane Hallegatte, Damon Matthews, Raya Muttarak, Dáithí Stone and the other, anonymous, reviewer(s) for their contribution to the peer review of this work.

**Reprints and permissions information** is available at <http://www.nature.com/reprints>.

# 文章

脆弱性提供有关当前适应的相关信息  
当地人口的潜力。

我们预处理GDP和GRDI产品可以使它们与在出生年份中的ULE估计值进行比较。对于GDP，与我们的分析中的其他数据集类似，我们将系列延长至2113，以通过复制原始数据集的最后一年来适应2020年出生队列的最长预期寿命。然后，我们使用Isimip人口总数按网格量表计算人均GDP。使用GDP人均大都会大会，我们使用1960 - 2020年出生队列的预期寿命信息来计算寿命平均人均GDP。我们将终身平均GDP人均GDP称为简单的GDP。对于grdi，我们将的原始网格单元格留在1 km上，以0.5°iSimip网格。尽管GRDI是由2010- 2020年数据组成的地图，但我们假设这是2020年的代表，但仍将其与1960- 2020年的出生队列范围进行比较，与其他分析相似。

然后，我们确定每个出生年份的生命周期GDP和单一的GRDI地图（假定与2020个人口一致的一致），我们确定20%的分位数（即（0-20]，（20-40），…（80-100））。为此，我们将这些脆弱性指标与我们的出生群体相同，以相同的范围为例。2020年的GDP与2020年的新生儿人口保持一致。最后，我们将其相关人口的排名漏洞指标分为几个几乎平等的人口，因为不可能实现完美的垃圾尺寸，因为该组的数量和最不足的范围是量身定做的。然后，可用于掩盖ULE的现有位置的地图，例如出生年和所有GMT途径。

- 31。Jones, C. D. Et al. CMIP5百年仿真的HADGEM2-ES实施。 *Geosci. Model Dev.* 4, 543–570 (2011)。 32. Dufresne, J.-L. et al. 使用IPSL-CM5接地系统模型的气候变化投影：从CMIP3到CMIP5。 *Clim. Dyn.* 40, 2123–2165 (2013)。 33. Watanabe, M. Et al. MIROC5改善气候模拟：平均状态，可变性和气候灵敏度。 *J. Clim.* 23, 6312–6335 (2010)。 34. Russo, S., Sillmann, J., & Fischer, E. M. 自1950年以来的十大欧洲热浪及其在未来几十年中的发生。 *Environ. Res. Lett.* 10, 124003 (2015)。 35. Russo, S., Sillmann, J., & Sterl, A. 在不同变暖水平的潮湿热浪。 *Sci. Rep.* 7, 7477 (2017)。 36. Yamazaki, D., Kanae, S., Kim, H., & Oki, T. 全球河流路由模型中基于物理的洪泛区淹没动力学的描述。 *Water Resour. Res.* 47, W04501 (2011)。 37. Emanuel, K. 缩小CMIP5气候模型显示21世纪的热带气旋活动增加。 *Proc. Natl Acad. Sci. USA* 110, 12219–12224 (2013)。 38. Holland, G. 修订后的飓风压力风模型。 *Mon. Weather Rev.* 136, 3432–3445 (2008)。 39. KleinGoldewijk, K., Beusen, A., & Janssen, P. 全球人口和建筑区域的长期动态建模以空间明确的方式：Hyde 3.1。 *Holocene* 20, 5 65–573 (2010)。 40. KleinGoldewijk, K., Beusen, A., & Drecht, G. V. Hyde 3.1在过去12, 000年中，人类引起的全球土地利用变化的空间显式数据库。 *Global Ecol. Biogeogr.* 20, 73–86 (2011)。 41. Fricke, O. et al. 共享社会经济途径的标记量化2：21世纪的中间场景。 *Global Environ. Change* 42, 251–267 (2017)。 42. Samir, K. C. & Lutz, W. 共享社会经济途径的人类核心：所有国家/地区的年龄、性别和教育水平划分为2100。 *Global Environ. Change* 42, 181–192 (2017)。 43. Lutz, W., Goujon, A., Samir, K. C., Stonawski, M., & Stilianakis, N. (Eds) *Demographic and Human Capital Scenarios for the 21st Century: 2018 Assessment for 201 Countries* (欧盟出版社，2018年出版物办公室)。 44. 联合国经济和社会事务部。 *World Population Prospects 2019* (联合国，2019年)。 45. Byers, E. et al. AR6方案数据库v.1.1。 *Zenodo* <https://doi.org/10.5281/zenodo.7197970> (2022)。 46. Murakami, D. & Yamagata, Y. 对栅格的人口和GDP场景的估计，并具有显式统计缩减。 *Sustainability* 11, 2104 (2019)。 47. Bartram, L., & Roe, B. 依赖比率：有用的决策工具？ *Geriatr. Gerontol. Int.* 5, 224–228 (2005)。 48. Sharroff, D. et al. 1990年至2019年之间5岁以下死亡率的全球、区域和国家趋势，基于情景的预测至2030年：联合国机构间儿童死亡率估算的系统分析。 *Lancet Glob. Health* 10, 195–206 (2022)。 49. Smits, J. & Permanyer, I. 统治人类发展数据库。 *Sci. Data* 6, 190038 (2019)。 50. Laborde Debucquet, D., & Martin, W. 全球增长对农村贫困的影响。 *Agric. Econ.* 49, 325–336 (2018)。 51. Bruederle, A., & Hodler, R. 夜间灯光作为地方一级人类发展的代理。 *PLoS One* 13, e0202231 (2018)。

## 数据可用性

此分析的数据来自多个来源，并在此列出。在ISIMIP存储库中可访问模型输入，原始影响模型模拟和从ISIMIP2B以及GDP数据的后处理（后者作为派生的输出数据）以及GDP数据（<https://data.isimip.org>）。队列大小从维特根斯坦人口统计学和全球人力资本中心（<https://dataexplorer.witt-gensteincentre.org/wcde-v2>）获取。预期寿命数据来自联合国人口统计数据门户（<https://population.un.org/dataportal/home?df=10750103-F8FA-4A7E-BB6A-B0F151970005>）。从AR6场景探索器<sup>45</sup>（<https://doi.org/10.5281/Zenodo.7197970>）中提取全局平均温度。GRDI托管在NASA Earthdata平台（<https://doi.org/10.7927/3xxe-ap97>）上。该分析中的地图包含用自然地球制成的基本图信息（NaturalTh- Data.com）。

致谢我们感谢Potsdam气候影响研究所（PIK）对Isimip的协调，并为ISIMIP2B捐款的模块赛。我们感谢M. Andrijevic, C.-F. Schleussner和E. Byers关于本文的讨论。W.T.在欧盟的Horizon框架研究与创新计划（授予协议第101076909号；ERC合并者Grant Grant Lacrima）下，承认欧洲研究委员会（ERC）的资金。我们承认欧盟根据授予协议编号的进一步资金。101081369（Sparcle）。这项工作中使用的计算资源和服务由VSC（Flemish Super Computer Center）提供，该研究基金会（Flanders（FWO）（FWO）和Flemish政府资助，EWI。这项工作得到了Wellcome Trust 30949/Z/24/Z的支持。

作者贡献L. Grant帮助构思了这项研究，进行了分析并撰写了论文。W.T.帮助构思了研究并撰写论文。IV.帮助编码本分析的部分并撰写论文。L. Gudmundsson, E.F. 和S.I.S有助于产生分析的想法并策划论文。

竞争利益作者宣称没有竞争利益。

## 附加信息

补充信息在线版本包含<https://doi.org/10.1038/s41586-025-08907-1>的补充材料。信件和材料请求应拨给卢克·格兰特（Luke Grant）。同行评审信息Nature感谢Stephane Hallegatte, Damon Matthews, Raya Muttarak,

Dáithí Stone和其他匿名评论者对这项工作的同行评审的贡献。转载和权限信息可在<http://www.nature.com/reprints>上获得。

## 代码可用性

可以在GitHub（[https://github.com/vub-hydr/2025\\_grant\\_etal\\_nature/tree/main](https://github.com/vub-hydr/2025_grant_etal_nature/tree/main)）上找到此分析的代码。

30. Dunne, J. P. Et al. GFDL的ESM2全球耦合气候- 碳地球系统模型。 第一部分：物理公式和基线模拟特征。 *J. Clim.* 25, 6646–6665 (2012)。